



Promotional synergistic effect of Cu and Nb doping on a novel Cu/Ti-Nb ternary oxide catalyst for the selective catalytic reduction of NO_x with NH₃

Xiaoxiang Wang ^a, Yun Shi ^{a,b}, Sujing Li ^{a,*}, Wei Li ^a

^a Key Laboratory of Biomass Chemical Engineering of Ministry of Education, Institute of Industrial Ecology and Environment, College of Chemical and Biological Engineering, Zhejiang University, Hangzhou 310027, China

^b Institute of Environment Engineering, College of Environmental Science and Resource, Zhejiang University, Hangzhou 310058, China

ARTICLE INFO

Article history:

Received 9 March 2017

Received in revised form 27 July 2017

Accepted 5 August 2017

Available online 8 August 2017

Keywords:

Cu/Ti-Nb oxide catalyst

NH₃-SCR

Surface acidity

Redox capability

Reaction pathway

ABSTRACT

A series of Ti-Nb binary oxide were synthesized by co-precipitation as supports to prepare Cu/Ti-Nb mixed oxide catalysts through wetness impregnation. The novel catalyst 0.8%Cu/Ti₂NbO_x exhibited an excellent catalytic activity and N₂ selectivity with a broad operation temperature (250–425 °C) under a gas hourly space velocity (GHSV) of 177,000 h⁻¹ for the selective catalytic reduction of NO_x with NH₃. A series of analytical techniques including high resolution transmission electron microscopy (HRTEM), N₂-physisorption, X-ray diffraction (XRD), Laser Raman spectra (LRS), X-ray photoelectron spectroscopy (XPS), electron paramagnetic resonance (EPR), NH₃ temperature-programmed desorption (NH₃-TPD), H₂ temperature-programmed reduction (H₂-TPR) and in situ diffuse reflectance infrared Fourier transform spectroscopy (in situ DRIFTS) were used to investigate the correlations among catalyst structure, surface properties and catalytic performance. For the support Ti₂NbO_x, the specific surface area was larger than that of TiO₂, promoting the high dispersion of the active component. Also, the surface acid sites were increased by addition of niobium oxide species and the redox capability of the support was enhanced by doping copper species. Moreover, the introduction of copper species effectively enhanced the catalytic performance within 225–400 °C. The copper species mainly existed as isolated Cu²⁺ and non-isolated Cu⁺ and the isolated Cu²⁺ ions played a significant role in the high NH₃-SCR performance over 0.8%Cu/Ti₂NbO_x catalyst. Hydrothermal aging treatment experiment demonstrated that 0.8%Cu/Ti₂NbO_x catalyst had an excellent hydrothermal stability. In addition, water vapor or/and SO₂ had a slightly reversible inhibition influence on the catalytic performance over 0.8%Cu/Ti₂NbO_x, indicating that it was a promising candidate for NH₃-SCR catalyst in the future practical application. The reaction pathway over 0.8%Cu/Ti₂NbO_x catalyst followed both Eley-Rideal mechanism and Langmuir-Hinshelwood mechanism at 225 °C.

© 2017 Elsevier B.V. All rights reserved.

1. Introduction

As the atmospheric pollution is becoming more and more severe, it has attracted public awareness on environmental protection awareness. Nitrogen oxides (NO_x) are one of major air pollutants that could cause photochemical smog, acid deposition, nitrate aerosol, ozone depletion and greenhouse effect [1–3]. NO_x is mainly emitted from stationary sources and mobile sources [4,5]. Selective catalytic reduction of nitrogen oxides with ammonia (NH₃-SCR) is an effective technique that has been widely applied for the abatement of NO_x from coal-fired plants and stationary boilers.

V₂O₅-WO₃(MoO₃)/TiO₂ catalyst has been commercially used for NO_x abatement due to its excellent catalytic performance. However, there are still some drawbacks, such as a narrow reaction temperature window of 300–400 °C and the biological toxicity of V₂O₅ to environment and human being [6,7]. Hence, it is necessary to develop environmental-friendly catalysts as alternatives.

Recently, TiO₂-anatase as support for the selective reduction catalyst was investigated by many researchers because of its great SO₂ resistance [6,8,9]. However, pure TiO₂ is poorly active during the SCR reaction due to its weak acidity and poor redox ability [10]. Some modifications have been investigated to overcome these defects. The addition of metal elements was commonly used to increase the activity of TiO₂. Yao found that more Lewis acid sites and NH₄NO₂ species were formed on the surface of CuO/Ti_{0.95}Ce_{0.05}O₂ catalyst, resulting in the best NO conversion

* Corresponding author.

E-mail address: sujing-li@zju.edu.cn (S. Li).

of 90% within a reaction temperature of 250–275 °C [5]. Also, The Cu/Ti oxide catalyst for NH₃-SCR has also been investigated [11,12], and the highest activity was achieved at high temperature (about 300 °C) with an active temperature window of 340–440 °C at GHSV of 50,000 h⁻¹. Both of their reports showed an enhancement on the catalytic activity of TiO₂ with addition of Cu. However, these catalysts exhibited over 90% NO_x conversion and N₂ selectivity with a relatively narrow reacting temperature window under a comparatively low GHSV below 100,000 h⁻¹. Effects of the temperature window and GHSV on the NH₃-SCR activity of catalyst have been investigated [13,14]. And it was essential for the potential SCR catalyst with high activity under broad range of reaction temperature and high GHSV. So, more efforts must be made to develop novel TiO₂-based catalysts for the further industrial application.

The promoting effect of niobium oxides on catalytic reduction of NO_x has been frequently investigated over V₂O₅-Nb₂O₅/TiO₂ [15], Fe₂O₃-Nb₂O₅ [16], CeO₂-Nb₂O₅ [4], NbO_x-CeO₂-ZrO₂ [17], Mn₂NbO_x [18] catalysts due to its strong acidity. Also, copper species have been commonly used as the active species in SCR catalysts for their low cost, non-toxicity and good catalytic activity [19]. Cu/SSZ-13 has been commercially used as the diesel exhaust denitration catalyst since 2010 [20,21]. Moreover, many researchers pointed that the catalytic activity was significantly affected by the dispersion of copper species on the support [5,19,22]. Well dispersion of active species would lead to a higher activity. Shan et al. [13] and Yao et al. [5] reported that addition of some elements (such as W or Ce) on the support could facilitate the dispersion of active species to increase the catalytic activity. The effects of niobium oxides on the dispersion of copper species as active species on the support TiO₂ have not been investigated at present.

In this study, niobium oxide was employed for enhancing the acidity of anatase TiO₂, and the copper species were used as mainly active species. The Cu/Ti-Nb ternary oxide catalyst was studied systematically. The optimal proportion of Cu/Ti-Nb has been explored. Meanwhile, the relationship among the "performance – structure – property" was investigated. Besides, *in situ* DRIFTS were performed to elucidate the mechanism of NH₃-SCR reaction over the catalyst in this work.

2. Experimental

2.1. Catalyst preparation

The titanium-niobium oxides were prepared by using co-precipitation method. Aqueous solutions of TiOSO₄·xH₂SO₄·xH₂O and NbCl₅ were mixed with the desired molar ratios. Sodium dodecyl benzene sulfonate and urea solution were then added into the mixed solution. Afterwards, the mixed solution was heated to 95 °C and held for 3 h under continuous magnetic stirring. The resulting suspension was naturally cooled down to room temperature and kept for 3 h and then centrifuged, washed with ultrapure water until no SO₄²⁻ and Cl⁻ were detected. Then the precipitate was washed twice with anhydrous ethanol and dried at 85 °C overnight. The resulting product was subsequently calcined in air at 350 °C for 1 h and 600 °C for 3 h and finally ground into a fine powder. The mixed oxides were denoted as Ti_mNb_nO_x, where m/n represents the molar ratio of Ti/Nb (m/n = 1, 2, 3, 4). The single oxides, namely Nb₂O₅ and TiO₂, were prepared by using precipitation method.

The yCu/Ti_mNb_nO_x samples were prepared by incipient-wetness impregnating the Ti_mNb_nO_x with Cu(NO₃)₂·3H₂O solution, where y indicated the loading amount of copper. For example, 1%Cu/Ti_mNb_nO_x catalyst represents that the copper loading amount is 1 g Cu/(1 g Cu + 99 g Ti_mNb_nO_x). The mixture was kept under stirring for 4 h and dried at 85 °C overnight. The obtained materials were calcined in the following air at 550 °C for 4 h. Fur-

thermore, yCu/TiO₂ catalysts were also prepared by using the same method for comparison.

2.2. Catalytic performance measurements

The catalytic performance of these catalysts for NH₃-SCR was determined under a steady state, involving a feed stream including 500 ppm NH₃, 500 ppm NO, 5% O₂, 50 ppm or 250 ppm SO₂(when used), 5% or 10% H₂O (when used), and N₂ as balance gas. 0.1–0.15 g catalysts of 40–60 mesh were placed between plugs of glass wool in a fixed bed quartz tube reactor (inner diameter = 0.6 cm) under atmospheric pressure. The reactor was placed inside a temperature-controlled furnace and a K-type thermocouple was inserted in the center of the catalyst bed for measuring the reaction temperature. Prior to catalytic tests, the catalysts were pretreated in a flow of 10% O₂/N₂ at 500 °C for 30 min to remove the residual species adsorbed on the surface and then cooled down to room temperature. After that, the simulated gas stream was fed into the reactor with a space velocity (GHSV) of 177,000 h⁻¹. The concentrations of outflow were measured by a Nicolet iS50 FTIR spectrometer equipped with a heated gas cell (Pike Technologies, optical path length = 2.4 m), which was kept 110 °C to avoid condensation during the tests. The spectra were recorded with a 0.5 cm⁻¹ resolution and co-addition of 32 scans, referenced to a N₂ background. For each experiment, fresh catalysts were used and the NO_x conversion and N₂ selectivity were calculated from the following equations:

$$\text{NO}_x \text{ conversion} = \frac{C_{\text{NO}_x(\text{in})} - C_{\text{NO}_x(\text{out})}}{C_{\text{NO}_x(\text{in})}} \times 100\% \quad (1)$$

$$C_{\text{NO}_x} = C_{\text{NO}} + C_{\text{NO}_2} + 2C_{\text{N}_2\text{O}} \quad (2)$$

$$\text{N}_2 \text{ selectivity} = \left(1 - \frac{2 \times C_{\text{N}_2\text{O}}}{C_{\text{NO}_x(\text{in})} + C_{\text{NH}_3(\text{in})} - C_{\text{NO}(\text{out})} - C_{\text{NO}_2(\text{out})} - C_{\text{NH}_3(\text{out})}} \right) \times 100\% \quad (3)$$

2.3. Catalysts characterization

The micro-morphology of the samples was characterized by high resolution transmission electron microscopy (HRTEM, JEOL JEM-2100F, Japan) operated at 200 kV. And the chemical analysis was obtained by energy dispersive X-ray spectrometer (EDS).

Textural characteristics of these catalysts were measured by N₂ adsorption-desorption experiment using a Micromeritics 3Flex instrument at liquid N₂ temperature (-196 °C). Prior to each analysis, the samples were outgassed under vacuum at 150 °C for 12 h. The specific surface areas were calculated by the Brunauer-Emmett-Teller (BET) equation at p/p₀ in the range of 0.05–0.30. Pore size distributions and average pore diameters were determined by Barrett-Joyner-Halenda (BJH) method using the desorption branches in 0.01–0.995 partial pressure range.

Powder X-ray diffraction (XRD) patterns of samples were carried out using a X-ray diffractometer (PANalytical X'Pert PRO, Holland) with Cu-K α radiation ($\lambda = 0.15406$ nm) at 40 kv and 40 mA. The X-ray diffractogram was recorded in a 2θ range of 10°–90° with the step size of 0.026°.

Laser Raman spectra (LRS) were collected on a Lab. HR800 Laser Raman spectrometer (Jobin Yvon Co., France) with a shot of LMPlanFI 50*/0.50 JAPAN using Ar⁺ laser beam. A wavelength of 514.532 nm was used for the exciting source and the laser power was 10 mW. The wavenumber values of the spectra were accurate to 1 cm⁻¹. And the samples were grounded before every measurement.

X-ray photoelectron spectroscopy (XPS) data were obtained with experiments on Thermo Scientific Escalab 250Xi instrument

equipped with an Al K α X-ray source ($h\nu = 1486.6\text{ eV}$) at a pass energy of 30 eV. Before the measurement, the sample was outgassed at room temperature. The base pressure was approximately $3 \times 10^{-9}\text{ mbar}$. Binding energies of Ti 2p, Nb 3d, Cu 2p, O 1s were calibrated using C 1s peak at 284.8 eV from carbon impurities. The resolution of the instrument enables peaks to be resolved within 0.45 eV from each other.

Electron paramagnetic resonance (EPR) experiments were conducted on a Bruker A300 EPR Spectrometer. About 20 mg powder samples were contained in a quartz tube with OD of 1.5 mm. The microwave power was 0.2 mW. The frequency was 9.436 GHz. The center field was 3400 G and the sweep width was 3000 G. The field was modulated with 4.00 G. A time constant of 10.24 msec was used. The conversion time was 20 msec. The EPR spectroscopy was recorded at 110 K to freeze copper ion mobility, under which the signal loss would be avoided due to the Cu–Cu dipolar interactions [23]. All the samples were fully hydrated by being saturated with moisture in the air [24].

Temperature programmed reduction of hydrogen (H₂-TPR) experiments were performed on Micromeritics AutoChem II 2920. Prior to the reduction, the sample (30 mg) was pretreated in a purified He stream at 350 °C for 1 h and then cooled down to 50 °C. And the reduction of samples was initiated from 50 °C to 1000 °C, with a mixture of 10% H₂/Ar (30 mL min⁻¹) at a rate of 10 °C min⁻¹. The interference of H₂O was eliminated by using a cold trap. And the consumption of H₂ was continuously monitored by a thermal conductivity detector (TCD).

NH₃-temperature programmed desorption (NH₃-TPD) experiments were carried out on Micromeritics AutoChem II 2920 with a quartz U-tube reactor. The signals of NH₃ were recorded by quadrupole mass spectrometer (QIC-20). Prior to the experiment, about 30 mg sample was pretreated at 500 °C for 1 h in a flow of high purified Helium (30 mL min⁻¹). Then the sample was cooled down to 100 °C and exposed to 10% NH₃/He (30 mL min⁻¹) until adsorption equilibrium, followed by purging with Helium (30 mL min⁻¹) at 100 °C for 2 h to remove physisorption of NH₃. Finally, the

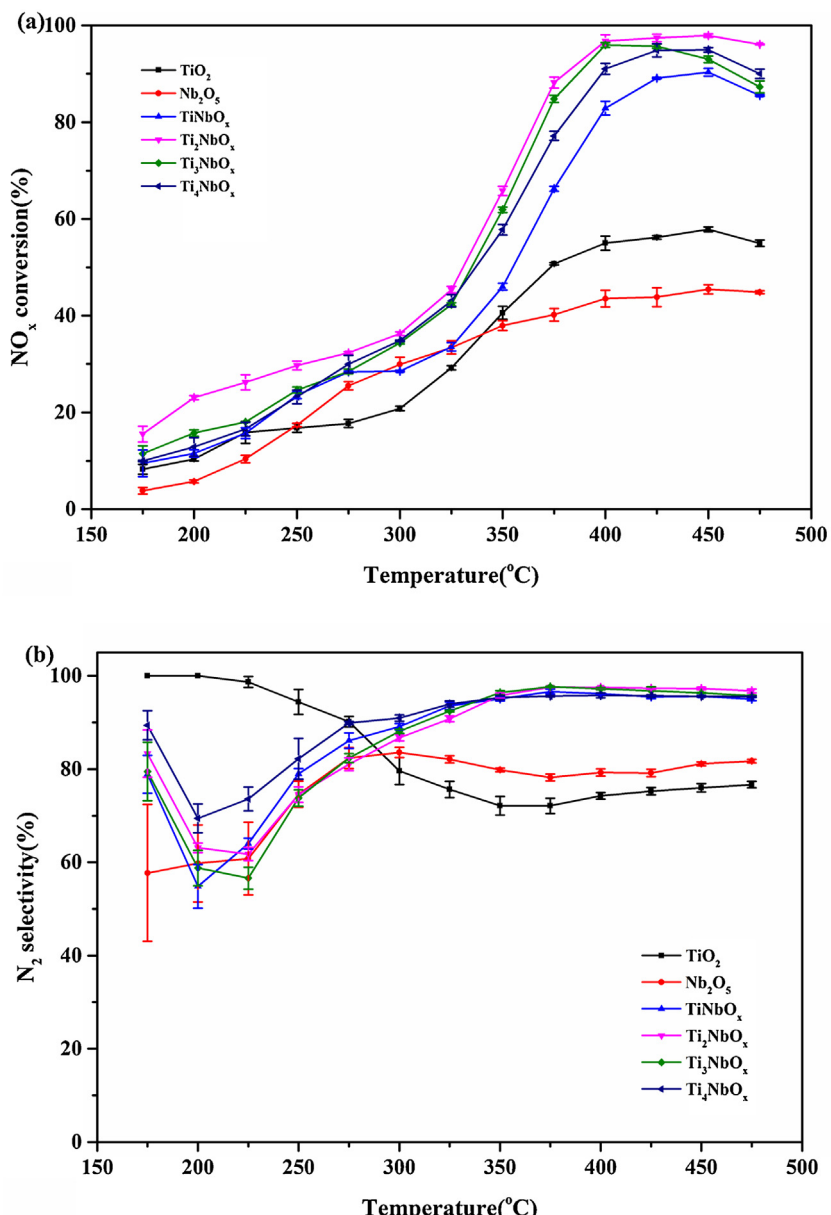


Fig. 1. (a) NO_x conversion and (b) N₂ selectivity over Ti_mNb_nO_x catalysts. Reaction conditions: [NH₃] = [NO] = 500 ppm, [O₂] = 5%, total flow rate = 500 mL min⁻¹, GHSV = 177,000 h⁻¹ and N₂ as balance.

sample was heated to 800 °C at a rate of 10 °C min⁻¹ in Helium (30 mL min⁻¹).

In situ diffuse reflectance infrared Fourier transform spectroscopy (in situ DRIFTS) experiments were carried out using a Fourier transform infrared spectrometer (FTIR, Nicolet NEXUS 6700) equipped with a MCT/A detector cooled by liquid N₂. The spectra were recorded in the range of 4000–650 cm⁻¹ at a spectral resolution of 4 cm⁻¹ (number of scans, 64). The DRIFTS cell (Harrick) was fitted with a KBr window and a heating cartridge which allowed the sample to be heated to 350 °C. The sample was pre-treated at 350 °C for 30 min in N₂ with a flow of 100 mL min⁻¹ before each experiment. The sample background of each target temperature was collected during the cooling process. For the NH₃ desorption experiment, the samples were exposed to a stream of 1000 ppm NH₃/N₂ (100 mL min⁻¹) for 1 h to be saturated at 100 °C and then purged with N₂ (100 mL min⁻¹) for 30 min to eliminate the gaseous and weakly adsorbed NH₃ molecules. Afterwards, the spectra were collected at various target tem-

perature at a rate of 10 °C min⁻¹ from 100 °C to 350 °C. For the reaction experiment, the samples were exposed to a stream of 1000 ppm NH₃/N₂ (100 mL min⁻¹) or 1000 ppm NO/N₂ + 5% O₂ (by volume) (100 mL min⁻¹) for 1 h to be saturated at 225 °C and then purged with N₂ (100 mL min⁻¹) for 30 min. Then the feeding gas of 1000 ppm NO/N₂ + 5% O₂ (by volume) (100 mL min⁻¹) or 1000 ppm NH₃/N₂ + 5% O₂ (by volume) (100 mL min⁻¹) was continuously introduced to the N₂-purged sample. All the IR spectra were recorded by subtraction of the corresponding background reference.

3. Results and discussion

3.1. Catalytic performances

3.1.1. NH₃-SCR activity of Ti_xNb_yO_z

The catalytic activities of the samples with different Ti/Nb molar ratios (1:0, 0:1, 1:1, 2:1, 3:1 and 4:1) were tested in the temperature

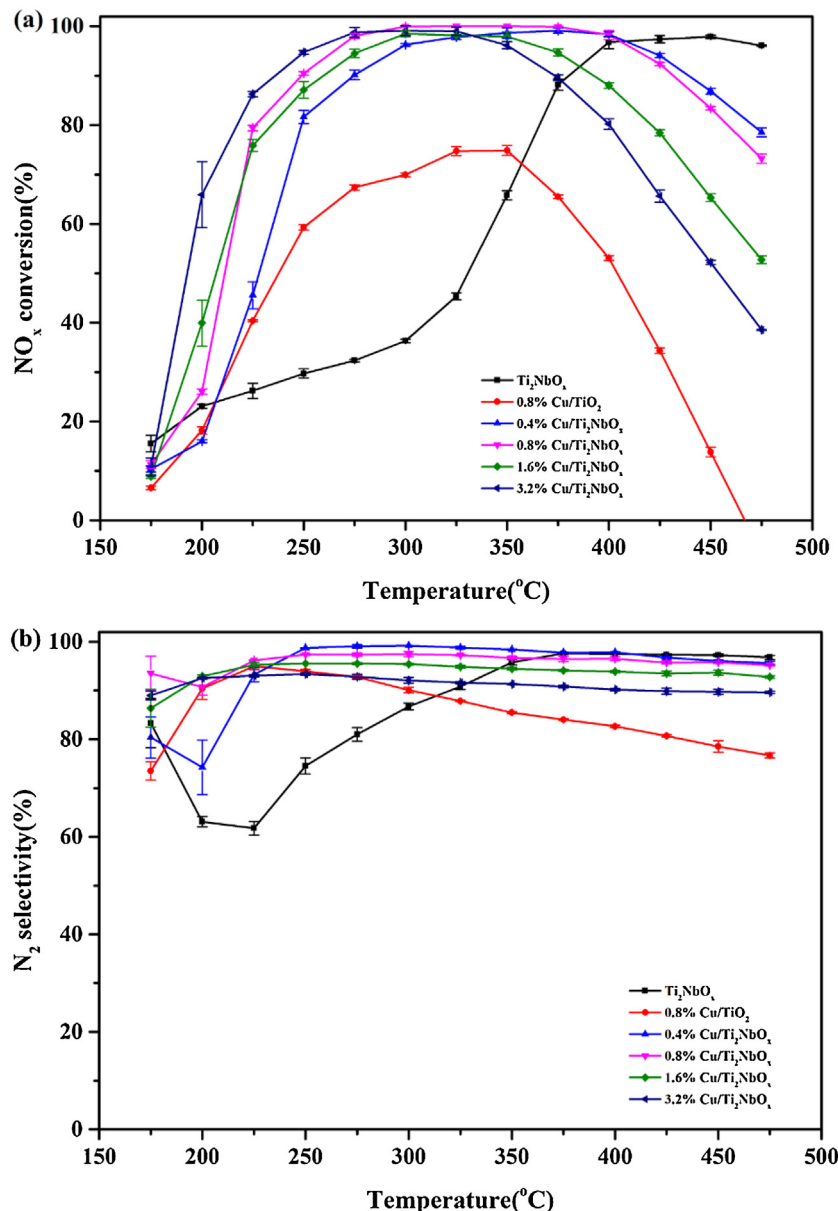


Fig. 2. (a) NO_x conversion and (b) N₂ selectivity over Cu/Ti₂NbO_x and Cu/TiO₂ catalysts. Reaction conditions: [NH₃] = [NO] = 500 ppm, [O₂] = 5%, total flow rate = 500 mL min⁻¹, GHSV = 177,000 h⁻¹ and N₂ as balance.

range of 175–475 °C. As shown in Fig. 1, single metal oxides (TiO_2 and Nb_2O_5) showed poor activities, with the maximum NO_x conversion of about 55% and 45%, respectively. Upon addition of Nb_2O_5 to TiO_2 , an increase in the NO_x conversion within the whole temperature range of 175–475 °C was observed. With the Ti/Nb ratio as 2:1, it showed the highest the NO_x conversion of above 95% in the temperature of 375–475 °C. Then, with the Ti/Nb ratio increasing to 3:1 and 4:1, the NO_x conversion started decreasing in the whole reaction temperature range. Hence, the Ti_2NbO_x showed the optimal activity. As for the $\text{Ti}_m\text{Nb}_n\text{O}_x$ support, similar tendencies with NO_x conversion and N_2 selectivity (as shown in Fig. 1b) were obtained. It showed a higher NO_x conversion in the temperature range of 400–450 °C. However, the activity of $\text{Ti}_m\text{Nb}_n\text{O}_x$ below 400 °C was still unsatisfactory. Considering the N_2 selectivity, TiO_2 showed a decreasing tendency with the elevation of temperature, in accordance with previous study [5]. In contrary, N_2 selectivity of Nb_2O_5 was increased with the increase of the temperature. Moreover, the addition of Nb_2O_5 resulted in the enhancement of N_2 selectivity for $\text{Ti}_m\text{Nb}_n\text{O}_x$, especially in the temperature range of 300–475 °C. And

the N_2 selectivity reached to 96% in the range of 350–475 °C over the $\text{Ti}_m\text{Nb}_n\text{O}_x$. The results of catalytic activity and selectivity implied that Nb_2O_5 could enhance the NO_x conversion and N_2 selectivity of TiO_2 efficiently in the higher temperature range of 300–475 °C and Ti_2NbO_x exhibited the best NH_3 -SCR activity among all the $\text{Ti}_m\text{Nb}_n\text{O}_x$.

3.1.2. Effect of Cu doping on NH_3 -SCR activity of $\text{Ti}_m\text{Nb}_n\text{O}_x$

A serial of yCu/ Ti_2NbO_x catalysts were synthesized and the catalytic performance of the samples for NH_3 -SCR of NO were given in Fig. 2. It was obvious that NO_x conversion and N_2 selectivity of Ti_2NbO_x were enhanced with addition of copper species within the temperature of 200–400 °C. With the increase of copper doping mass ratio from 0.4% to 3.2%, the high temperature (350–475 °C) NO_x conversion decreased while the low temperature (175–300 °C) NO_x conversion was increased. Furthermore, the activities of these catalysts exhibited a similar trend. They firstly increased up to a maximum value with the elevation of temperature from 175 °C to about 300 °C, and were maintained at the maximum at a cer-

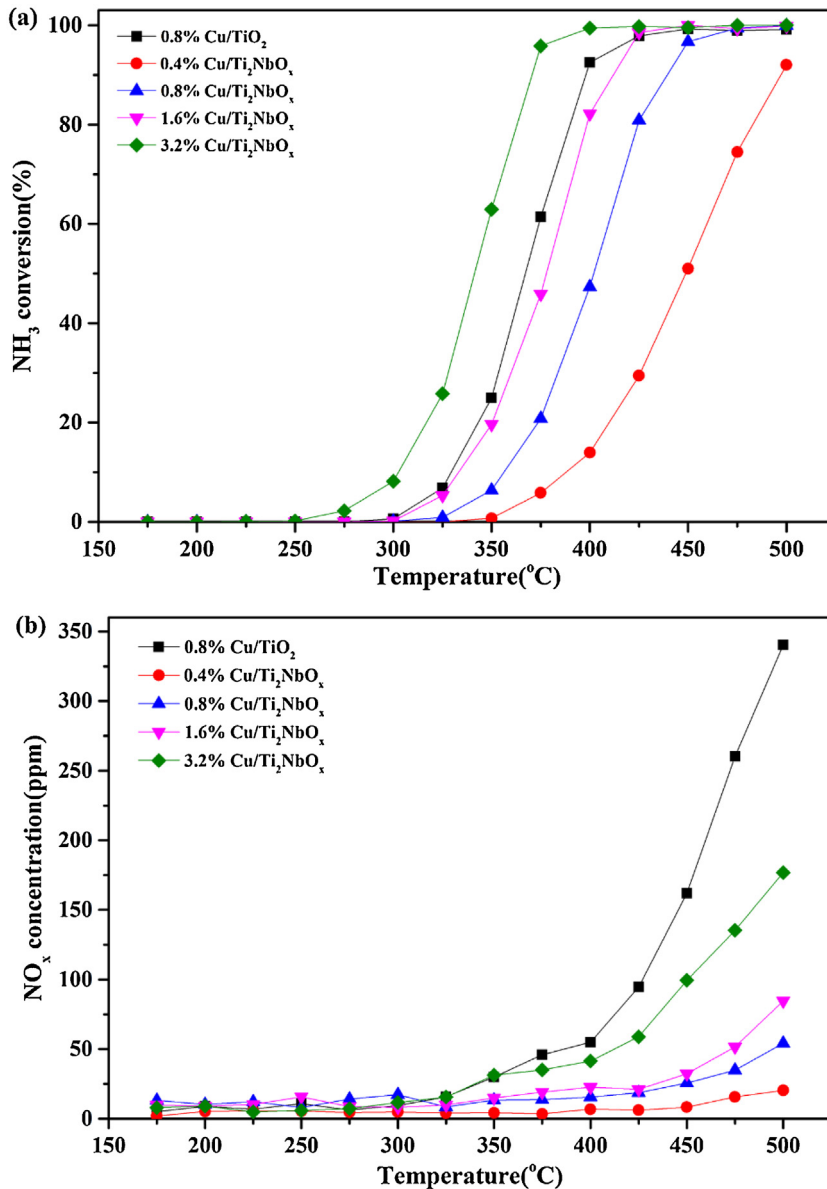


Fig. 3. (a) NH_3 conversion and (b) NO_x concentration over Cu/Ti₂NbO_x and Cu/TiO₂ catalysts. Reaction conditions: $[\text{NH}_3] = 500 \text{ ppm}$, $[\text{O}_2] = 5\%$, total flow rate = 500 mL min^{-1} , GHSV = $177,000 \text{ h}^{-1}$ and N_2 as balance.

tain temperature of 300–375 °C then decreased with the further increase of temperature in the range of 375–475 °C. Copper species was common used as an active component for SCR catalysts in the low temperature range in the literature [5,25,26]. However, the decreasing NO_x conversion upon 400 °C should be related to the unselective oxidation of NH₃ [27,28]. In addition, with the increase of copper content, the NO_x conversion decreased more distinctly within the high temperature, which might be related to the incremental extent of the NH₃ unselective oxidation. So, NH₃ oxidation experiments were conducted to illustrate the issue. And the results were given in Fig. 3. The NH₃ oxidation began at 275 °C and the NH₃ conversion increased up to about 99% with

the elevating temperature. Meanwhile, NO_x was generated and increased gradually. The NO_x conversion decreased at temperature above 400 °C (Fig. 2), while the NH₃ conversion increased to 99% (Fig. 3). The competitive consumption of NH₃ and the production of NO_x might lead to the decrease of the NH₃-SCR activity in the high temperature [29,30]. It was obvious that NH₃ oxidation and NO_x productions increased with the increment of copper content. The NO_x production of 0.4%Cu/Ti₂NbO_x was 20 ppm while it was 177 ppm for 3.2%Cu/Ti₂NbO_x. Compared with yCu/Ti₂NbO_x catalysts, 0.8%Cu/TiO₂ showed a higher NH₃ conversion and largest NO_x production. From the NH₃-SCR activity results and NH₃ oxidation activity results, we could conclude that the decrease of NH₃-SCR

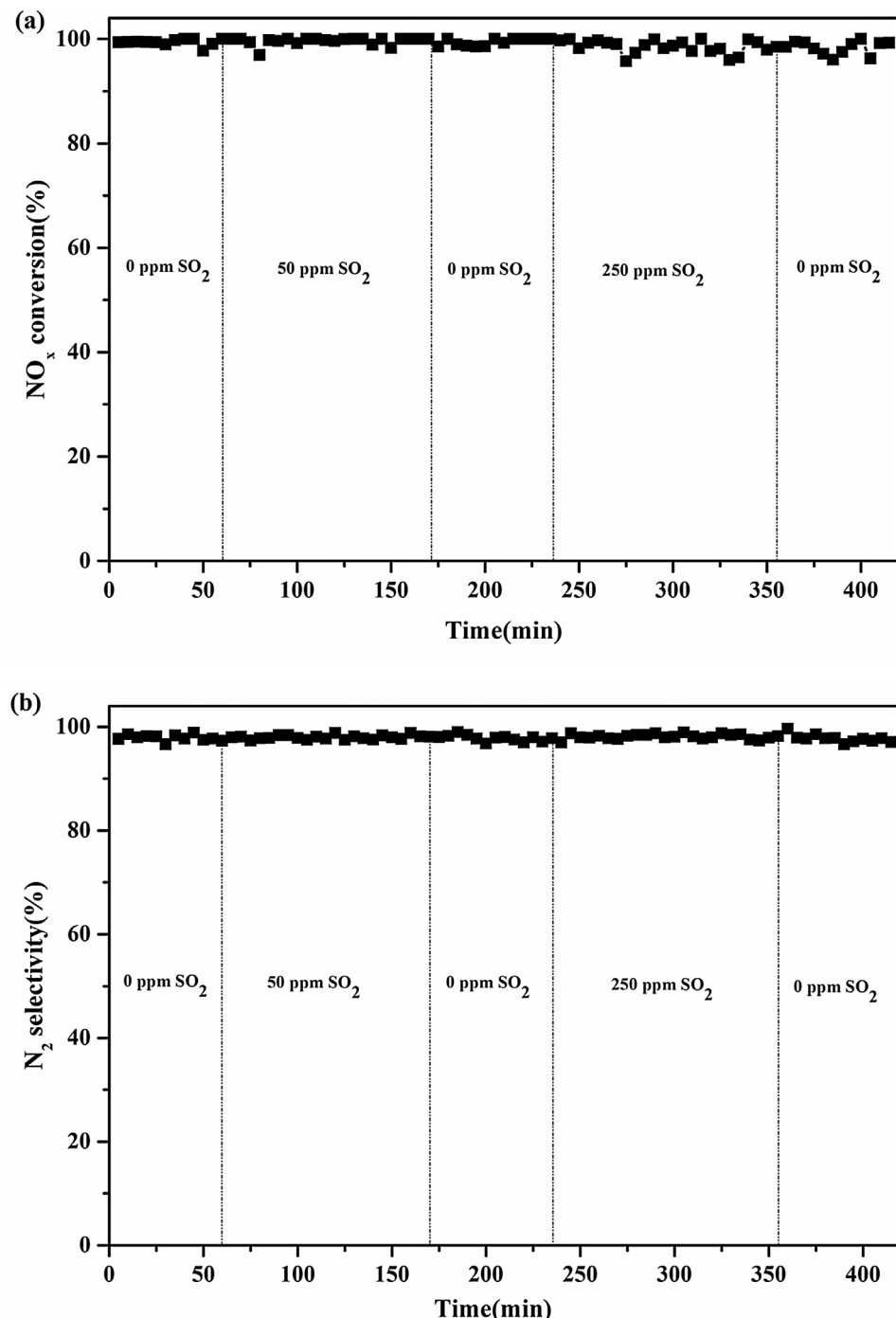


Fig. 4. Effect of SO₂ on the (a) NO_x conversion and (b) N₂ selectivity over 0.8%Cu/Ti₂NbO_x catalyst at 325 °C. Reaction conditions: [NH₃] = [NO] = 500 ppm, [O₂] = 5%, 50–250 ppm SO₂ (when used), total flow rate = 500 mL min⁻¹, GHSV = 177,000 h⁻¹ and N₂ as balance.

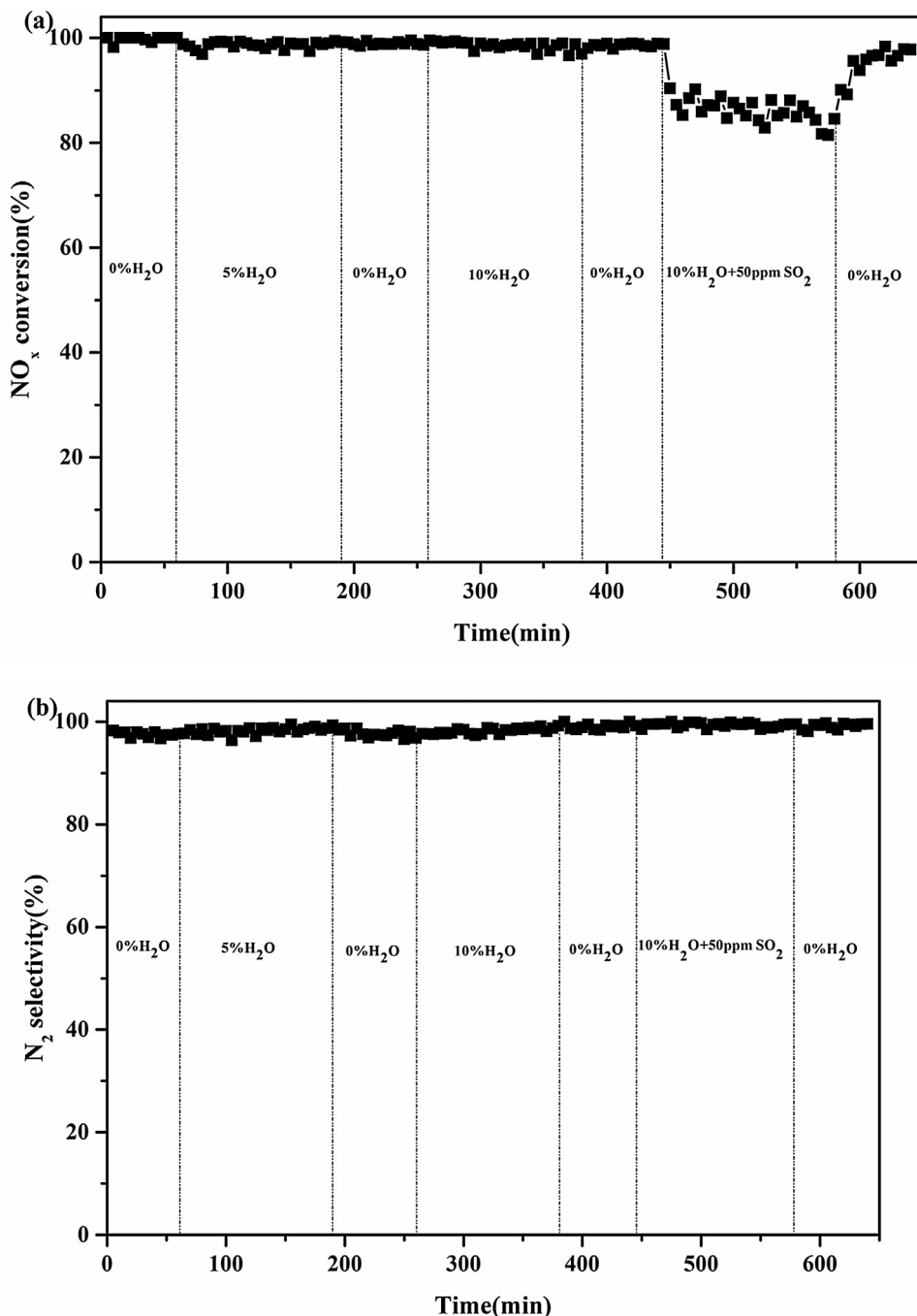


Fig. 5. Effect of H_2O and H_2O+SO_2 on the (a) NO_x conversion and (b) N_2 selectivity over $0.8\%Cu/Ti_2NbO_x$ catalyst at $325^\circ C$. Reaction conditions: $[NH_3]=[NO]=500\text{ ppm}$, $[O_2]=5\%$, $50\text{ ppm } SO_2$ (when used), $5\%-10\% H_2O$ (when used), total flow rate = 500 mL min^{-1} , GHSV = $177,000\text{ h}^{-1}$ and N_2 as balance.

activity at high temperature was mainly due to NH_3 oxidation and that the copper content had a significant effect on the NH_3 oxidation activity. Increase of copper species content would facilitate the NH_3 oxidation.

Compared with $0.8\%Cu/TiO_2$, the yCu/Ti_2NbO_x showed higher activity and selectivity in a wide temperature range of $275\text{--}425^\circ C$, indicating that some promotional synergistic effect between Cu and Nb species might exist in the yCu/Ti_2NbO_x catalysts. With Cu loading amount increased from 0.4% to 0.8% , the increased NO_x conversion at a broad operation temperature window was observed. But further increasing the Cu loading amount to 3.2% , the operation window was shrunken slightly and the N_2 selectivity declined. Among all the catalysts, $0.8\%Cu/Ti_2NbO_x$ exhibited the highest

NH_3 -SCR activity at the temperature of $250^\circ C\text{--}425^\circ C$, in which the NO_x conversion was maintained upon 90% and the N_2 selectivity was about 97% with a GHSV of $177,000\text{ h}^{-1}$. This suggested that 0.8% was the optimal mass ratio of Cu doping.

3.1.3. Effect of H_2O and SO_2 on the SCR activity of $0.8\%Cu/Ti_2NbO_x$

Water vapor and SO_2 are present in the exhaust gas and would influence the catalytic activity. It is necessary to investigate the H_2O and SO_2 resistance of $0.8\%Cu/Ti_2NbO_x$ catalyst. The sulfur resistance of $0.8\%Cu/Ti_2NbO_x$ catalyst at $325^\circ C$ was evaluated in this work and the corresponding results were presented in Fig. 4. In the presence of $50\text{ ppm } SO_2$, there was almost no change on the NO_x conversion and N_2 selectivity. Moreover, the activity of

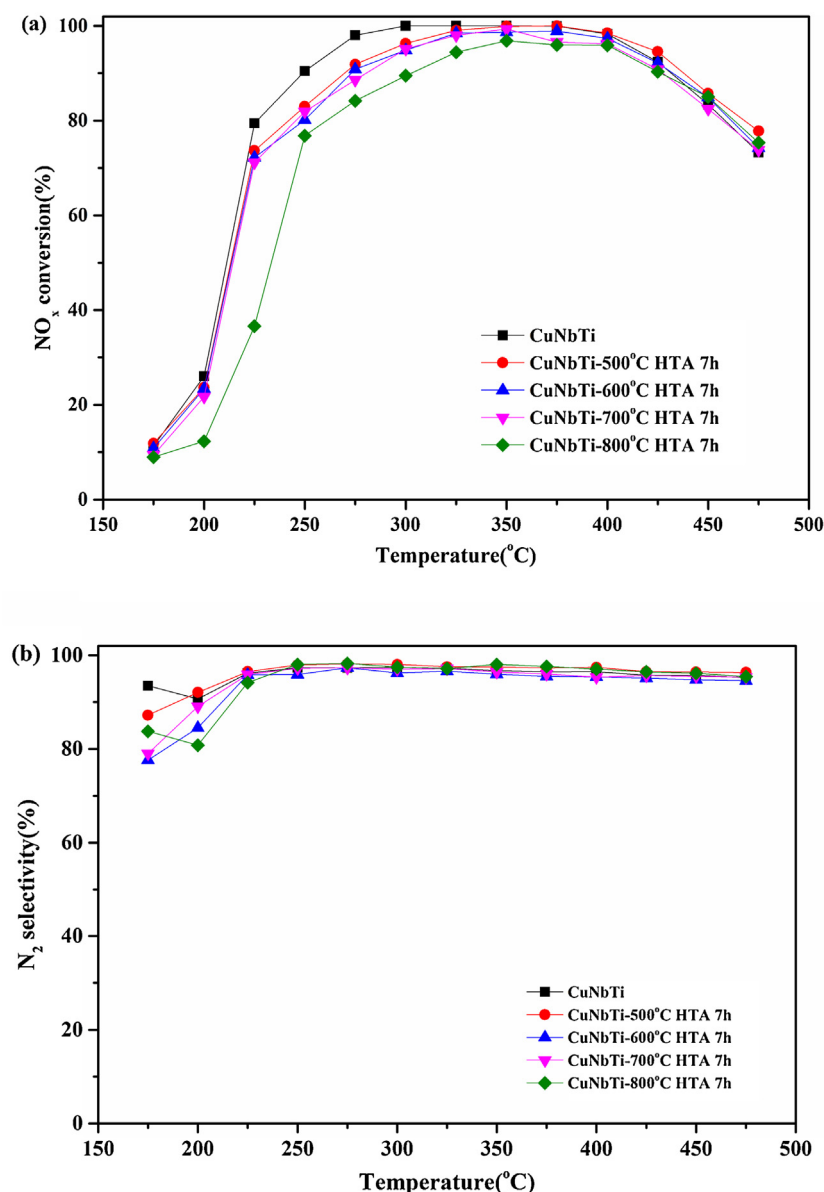


Fig. 6. (a) NO_x conversion and (b) N₂ selectivity over fresh 0.8%Cu/Ti₂NbO_x and after hydrothermal aged 0.8%Cu/Ti₂NbO_x catalysts. Reaction conditions: [NH₃] = [NO] = 500 ppm, [O₂] = 5%, total flow rate = 500 mL min⁻¹, GHSV = 177,000 h⁻¹ and N₂ as balance.

0.8%Cu/Ti₂NbO_x was maintained at nearly 100% with the addition of 250 ppm SO₂, indicating an excellent sulfur resistance of the catalyst. Interestingly, when only 5% or 10% H₂O was added in the feeding gas at 325 °C, the NO_x conversion and N₂ selectivity were stable with slight fluctuation, as shown in Fig. 5. However, the coexistence of 50 ppm SO₂ and 10% H₂O resulted in a decrease of NO_x conversion. And the NO_x conversion decreased to about 86% while the N₂ selectivity was maintained at above 98%. It was observed that there were some crystals forming on the catalyst after the reaction with H₂O and SO₂. Hence, it is assumed that the decrease of NO_x conversion might be mainly attributed to the deposition of ammonium sulfate, such as NH₄HSO₄ and (NH₄)₂S₂O₇ on the catalyst surface, blocking the active sites of catalysts [2,5,13]. After turning off H₂O and SO₂ in the feed stream, the NO_x conversion was restored to its original level gradually. This result showed that the coexistence of water vapor and SO₂ inhibited the catalytic activity and its inhibition effect was reversible. Nevertheless, the sole existence of water vapor or SO₂ would not pose any negative effect on the SCR activity.

3.1.4. The hydrothermal stability of 0.8%Cu/Ti₂NbO_x

To investigate the hydrothermal stability of 0.8%Cu/Ti₂NbO_x, the catalysts were heated to 500 °C, 600 °C, 700 °C, and 800 °C from 30 °C at a ramp rate of 10 °C min⁻¹, respectively. And then it was held in a mixture of 10% H₂O, 5%O₂ and N₂ as balance for 7 h at the corresponding final temperature. The hydrothermal aged catalysts were abbreviated as CuNbTi- \times HTA 7 h, where \times represented the hydrothermal aged temperature. The catalytic performances of these catalysts for NH₃-SCR were determined by the same method as described in Section 2.2.

Fig. 6 depicts the NO_x conversion and N₂ selectivity over 0.8%Cu/Ti₂NbO_x catalysts before and after hydrothermal aging under 500–800 °C. Hydrothermal aging treatment did not lead to a significant reduction of the catalytic activity and all of them exhibited a similar catalytic performance. Compared with fresh 0.8%Cu/Ti₂NbO_x catalyst, NO_x conversion of CuNbTi-500-HTA decreased by 7% in the temperature range of 225–300 °C. And the extent of activity decline increased with the rise of the temperature of hydrothermal aging. The NO_x conversion of CuNbTi-800-HTA

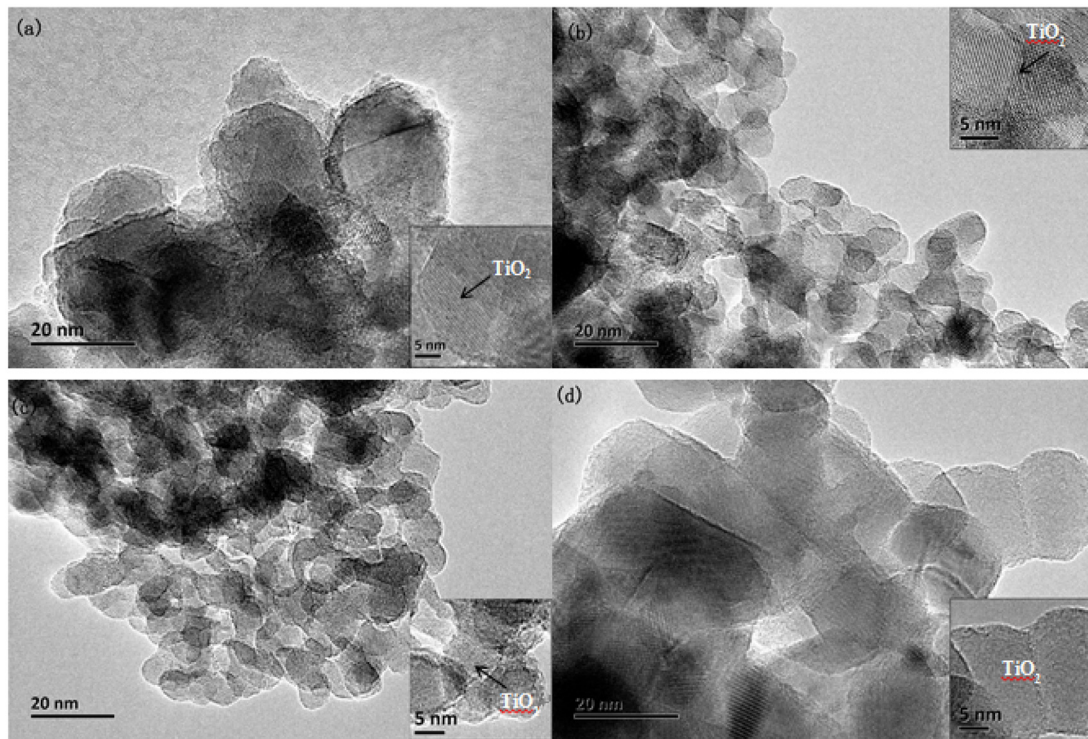


Fig. 7. TEM patterns of (a) TiO_2 , (b) Ti_2NbO_x , (c) 0.8%Cu/ Ti_2NbO_x and (d) 0.8%Cu/ TiO_2 .

catalyst decreased from 79% to 37% at 275 °C and it increased to 90% at 300 °C. Interestingly, the NO_x conversion of all aging catalysts kept upon 90% over 300 °C. Meanwhile, the hydrothermal aging treatment had little effect on the N_2 selectivity of 0.8%Cu/ Ti_2NbO_x and it was maintained over 90% from 225 °C to 475 °C. Both of NO_x conversion and N_2 selectivity demonstrated that 0.8%Cu/ Ti_2NbO_x catalyst had an excellent hydrothermal stability.

3.2. Physicochemical characterization

3.2.1. Micro-morphology of catalysts

The TEM patterns of TiO_2 , Ti_2NbO_x , 0.8%Cu/ Ti_2NbO_x and 0.8%Cu/ TiO_2 were shown in Fig. 7, which provided a view of the morphology of the catalysts. It was observed that all of them had oval-shaped crystal particles, suggesting to be anatase TiO_2 [31]. TiO_2 and 0.8%Cu/ TiO_2 showed larger grain size and the diameter was in the range of 22–29 nm. However, the grain size decreased with the addition of niobium oxides for Ti_2NbO_x and 0.8%Cu/ Ti_2NbO_x , whose diameters were in the range of 10–15 nm, indicating that the addition of niobium oxides promoted TiO_2 nucleation and reduced the grain size. This effect was favored to the dispersion of copper species. However, the niobium oxides and copper species were difficult to be observed in these patterns. To further investigate the dispersion of Ti, Nb and Cu elements over 0.8%Cu/ Ti_2NbO_x , EDS scan maps were conducted and the results showed that the copper species were well dispersed on the support, as presented in Fig. 1S.

Table 1

Structural parameters of catalysts measured by N_2 adsorption experiments and calculate from XRD experiments using Scherrer equation.

Samples	Surface area(m^2/g)	Total pore volume(cm^3/g)	Average pore diameter(nm)	Lattice parameter(Å)	Crystallite (nm)
TiO_2	13.0	0.06	7.2	3.738	22.6
Nb_2O_5	17.2	0.25	30.4	3.614	36.0
Ti_2NbO_x	84.7	0.45	14.5	4.144	10.9
0.8%Cu/ TiO_2	13.1	0.09	12.6	3.788	28.8
0.8%Cu/ Ti_2NbO_x	73.1	0.29	11.5	3.808	9.3

3.2.2. Structural and textural characteristics

The surface areas and pore characterization of TiO_2 , Nb_2O_5 , Ti_2NbO_x , 0.8%Cu/ TiO_2 and 0.8%Cu/ Ti_2NbO_x catalysts are summarized in Table 1. And the crystallite size of catalysts is calculated using the Scherrer equation. TiO_2 , Nb_2O_5 and 0.8%Cu/ TiO_2 have the surface areas of $13.0 \text{ m}^2/\text{g}$, $17.2 \text{ m}^2/\text{g}$ and $13.1 \text{ m}^2/\text{g}$, respectively. With the addition of Nb, the binary oxides Ti_2NbO_x has largest surface area of $84.7 \text{ m}^2/\text{g}$, followed by 0.8%Cu/ Ti_2NbO_x with a surface area of $73.1 \text{ m}^2/\text{g}$. This suggests that the addition of niobium oxides results in the increase of surface area, total pore volume and average pore diameter of the TiO_2 support, hence providing more surface active sites for the SCR reaction. However, the surface area of 0.8%Cu/ Ti_2NbO_x decreased with addition of 0.8% copper on Ti_2NbO_x . This could be ascribed to the blockage on pores due to impregnation of copper species [17]. But the activity of 0.8%Cu/ Ti_2NbO_x was better than Ti_2NbO_x , indicating some promotional synergistic effect existed between the Cu and Nb species. Nb species could increase the specific surface area of the support to promote the dispersion of Cu species while Cu species enhanced the catalytic activity of the support. Also, the lower surface area and pore volume of 0.8%Cu/ TiO_2 might be one of factors leading to a worse catalytic activity.

The powder XRD patterns of samples are displayed in Fig. 8. All the reflections of pure TiO_2 exhibited typical anatase TiO_2 diffraction patterns (PDF-ICDD 99-0008), which was favored for the activities of NH_3 -SCR catalysts [8,32]. Pure Nb_2O_5 showed niobium oxide structure (PDF-ICDD 28-0317) while anatase TiO_2 diffrac-

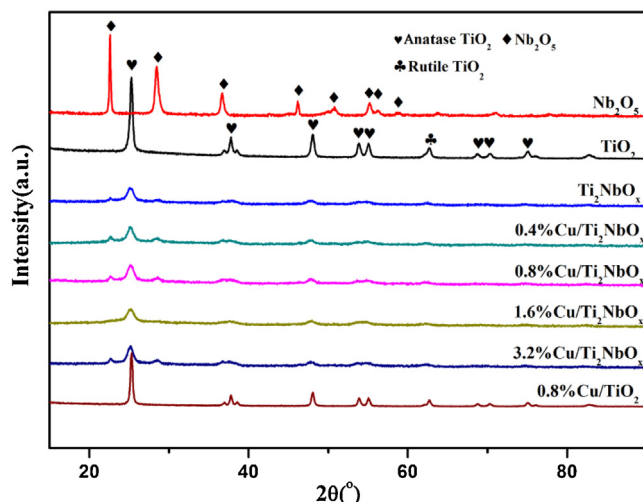


Fig. 8. XRD patterns of TiO_2 , Nb_2O_5 , Cu/TiO_2 and $\text{Cu}/\text{Ti}_2\text{NbO}_x$ catalysts.

tion peaks were observed in the spectra of Ti_2NbO_x . Moreover, the lattice parameter of Ti_2NbO_x was larger than that of anatase TiO_2 , which might because of the fact that the ionic radius of Nb^{5+} (0.64 \AA) was smaller than that of Ti^{4+} (0.68 \AA), and this would contribute to the incorporation of partial Nb^{5+} into the lattice of anatase TiO_2 , resulting in the expansion and distortion of the lattice [5,17]. Decrement of the crystallite size of Ti_2NbO_x indicated that the introduction of Nb^{5+} might inhibit the grain growing, which was in agreement with the results of TEM. Also, two weaker crystallization degree of Nb_2O_5 at 22.6° and 28.5° in the bulk phase of Ti_2NbO_x and $\text{yCu}/\text{Ti}_2\text{NbO}_x$ were observed while no copper species were detected in the $\text{yCu}/\text{Ti}_2\text{NbO}_x$, indicating that introduction of niobium oxide strongly inhibited the crystallization of anatase TiO_2 on the catalyst surface, probably leading to a much higher dispersion degree of active Cu species. After the loading of copper species, all of the $\text{yCu}/\text{Ti}_2\text{NbO}_x$ and $0.8\%\text{Cu}/\text{TiO}_2$ catalysts kept their original structure, and no additional diffraction peaks of crystalline CuO were observed, suggesting that copper species on the surface of supports were in the forms of highly dispersed state [5].

The Raman spectra were exhibited in Fig. 9. TiO_2 exhibited several Raman bands at around 145 cm^{-1} , 196 cm^{-1} , 395 cm^{-1} , 515 cm^{-1} , 636 cm^{-1} attributing to $E_{g(1)}$, $E_{g(2)}$, $B_{1g(1)}$, $A_{1g} + B_{1g(2)}$, and $E_{g(3)}$ vibration modes, respectively [5,33]. For niobium oxide, a band at 697 cm^{-1} was presented, suggesting the structure of niobium oxide was mainly octahedrally coordinated niobium oxide compound [4]. Also, the bands of Ti_2NbO_x were very similar with those of TiO_2 . But the intensity of peaks at 636 cm^{-1} for Ti_2NbO_x and $0.8\%\text{Cu}/\text{Ti}_2\text{NbO}_x$ was stronger than those for TiO_2 . It might be because the Raman band of niobium oxide at 697 cm^{-1} had an influence on the band of Ti_2NbO_x and $0.8\%\text{Cu}/\text{Ti}_2\text{NbO}_x$ at 636 cm^{-1} . The weak peaks at 697 cm^{-1} for Ti_2NbO_x and $0.8\%\text{Cu}/\text{Ti}_2\text{NbO}_x$ catalysts showed that there were also some intergrowth of TiO_2 and Nb_2O_5 . In addition, the bands of copper species were absent for those of $0.8\%\text{Cu}/\text{TiO}_2$ and $0.8\%\text{Cu}/\text{Ti}_2\text{NbO}_x$, indicating that copper species were in the forms of highly dispersed state, which was consistent

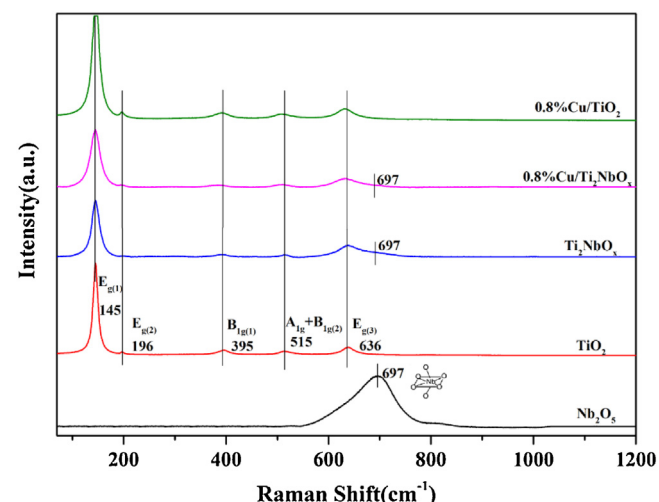


Fig. 9. Raman spectra of Nb_2O_5 , TiO_2 , Ti_2NbO_x , $0.8\%\text{Cu}/\text{Ti}_2\text{NbO}_x$ and $0.8\%\text{Cu}/\text{TiO}_2$ catalysts.

with the results of XRD and EDS. The results of XRD and Raman indicated that niobium oxide species existed in two states: some Nb^{5+} was into the lattice of TiO_2 while other niobium oxides were intergrowth with TiO_2 .

The chemical states of all the elements in the catalysts were analyzed by XPS technique. Fig. 10 displays the XPS spectra of $\text{Ti} 2p$, $\text{Nb} 3d$, $\text{Cu} 2p$ and $\text{O} 1s$ for different catalysts. The surface compositions of samples are summarized in Table 2. $\text{Ti} 2p$ spectra were presented in Fig. 10(a), which was consisted of two peaks($\text{Ti} 2p_{3/2}$ and $\text{Ti} 2p_{1/2}$). The binding energy peaks of $\text{Ti} 2p_{3/2}$ and $\text{Ti} 2p_{1/2}$ for TiO_2 at 458.98 eV and 464.67 eV were the characteristics of Ti^{4+} species [34]. The binding energy of $\text{Ti} 2p_{3/2}$ and $\text{Ti} 2p_{1/2}$ over Ti_2NbO_x located at 459.40 eV and 465.09 eV respectively were attributed to Ti^{3+} . The binding energy shifted to high direction when niobium oxides species doping, indicating that the interaction between TiO_2 and niobium oxides species was strong. It was shown by XRD that partial Nb^{5+} were incorporated into the lattice of TiO_2 , and the occupation of titanium sites by Nb^{5+} had an influence on the electrons distribution. Then electrons transfer was strengthen for titanium and the electrons around the titanium would be transferred to some active species under the effects of niobium oxides species [26], promoting the formation of Ti^{3+} . $\text{Ti} 2p$ peaks became broader for Ti_2NbO_x , showing a heterogeneous environment of Ti ions [35]. It was further found that a shift to lower binding energy occurred upon copper species doping for $0.8\%\text{Cu}/\text{TiO}_2$ and $0.8\%\text{Cu}/\text{Ti}_2\text{NbO}_x$ catalysts, implying a strong interaction between copper species and the supports contributed to the $\text{NH}_3\text{-SCR}$ activity [36]. On the one hand, copper doping could increase the electron density around the atoms over the surface of supports catalysts [33]. On the other hand, the redox cycle of $\text{Cu}^{2+} + \text{Ti}^{3+} \leftrightarrow \text{Cu}^+ + \text{Ti}^{4+}$ was established for $0.8\%\text{Cu}/\text{Ti}_2\text{NbO}_x$ catalyst, which would promote the activity of $\text{NH}_3\text{-SCR}$ [5].

Fig. 10(b) shows the XPS spectrum of $\text{Nb} 3d$ for Ti_2NbO_x and $0.8\%\text{Cu}/\text{Ti}_2\text{NbO}_x$. The peaks of $\text{Nb} 3d_{5/2}$ and $\text{Nb} 3d_{3/2}$ at 207.67 eV

Table 2
The surface compositions of the samples.

samples	Atom concentration (%)				Atom ratio(%)	
	Ti	Nb	O	Cu	$\text{O}_\alpha/(\text{O}_\alpha + \text{O}_\beta)$	$\text{Cu}^+/(\text{Cu}^+ + \text{Cu}^{2+})$
TiO_2	31.55	–	68.45	–	18.94	–
Ti_2NbO_x	18.10	11.68	70.22	–	24.07	–
$0.8\%\text{Cu}/\text{TiO}_2$	31.78	–	66.84	1.38	19.78	44.20
$0.8\%\text{Cu}/\text{Ti}_2\text{NbO}_x$	18.05	11.40	69.66	0.89	25.87	48.07

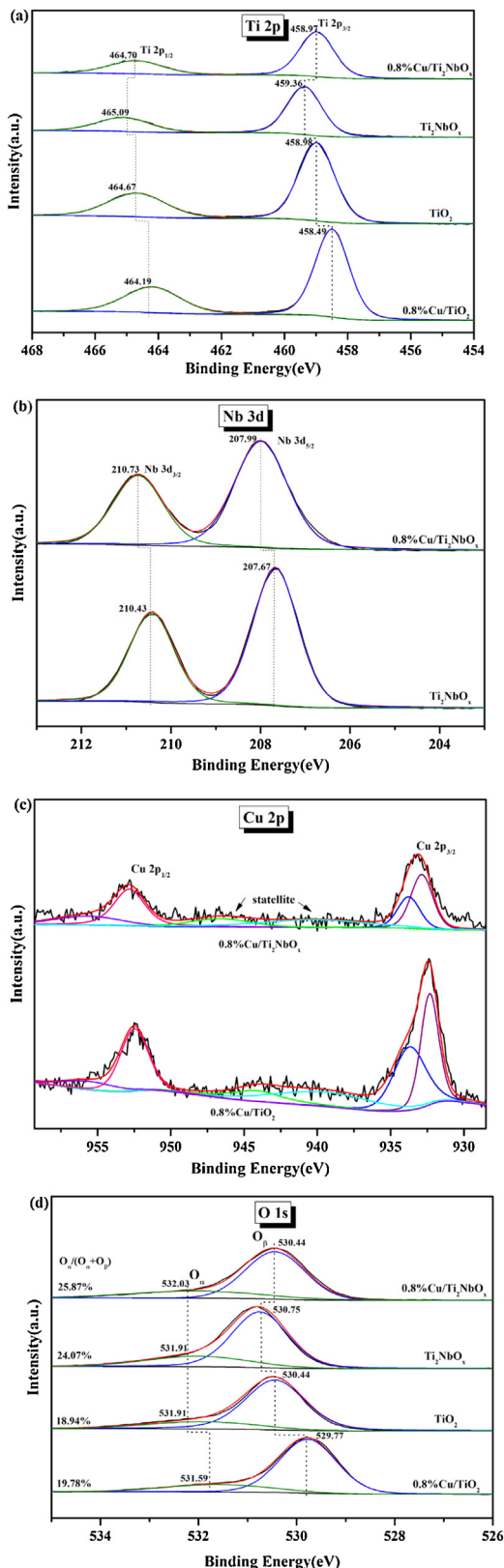


Fig. 10. XPS spectra of TiO₂, Ti₂NbO_x, 0.8%Cu/TiO₂ and 0.8%Cu/Ti₂NbO_x catalysts: (a) Ti 2p, (b) Nb 3d, (c) Cu 2p, and (d) O 1s.

and 210.43 eV were assigned to the Nb⁵⁺ species [4,17,31]. Compared with those of Ti₂NbO_x catalyst, the peaks shifted to higher binding energy when copper species were added, implying that copper species altered the chemical environment around the Nb⁵⁺ species. Both of Ti 2p and Nb 3d spectrums indicated that copper species had a strong interaction with the supports.

The Cu 2p spectra of 0.8%Cu/TiO₂ and 0.8%Cu/Ti₂NbO_x were shown in Fig. 10(c), which contained two main peaks of Cu 2p_{3/2} and Cu 2p_{1/2} and some satellite peaks within 935–950 eV being relevant to Cu²⁺ species [5]. Cu 2p_{3/2} split into two peaks that were located at 932.34–932.87 eV and 933.70–933.76 eV while the Cu 2p_{1/2} split into two peaks that were located at 952.48–952.82 eV and 955.58–955.70 eV. The binding energies at 932.34–932.87 eV and 952.48–952.82 eV were attributed to Cu⁺ while the peaks at about 933.70–933.76 eV and 955.58–955.70 eV were the characteristics of Cu²⁺ [5,34,37,38], indicating the existence of Cu²⁺ and Cu⁺ species over the catalysts. Furthermore, the Cu⁺ percent content was calculated by the area ratio between Cu⁺ and (Cu⁺ + Cu²⁺), as shown in Table 2. There was more Cu⁺ over 0.8%Cu/Ti₂NbO_x than 0.8%Cu/TiO₂, which was in agreement with the results of CO adsorption (Fig. 2S). And the Cu⁺ was mainly in the forms of non-isolated state. The increase of Cu⁺ content for 0.8%Cu/Ti₂NbO_x was mainly owing to the redox cycle of Cu²⁺ + Ti³⁺ ⇌ Cu⁺ + Ti⁴⁺ over the Ti₂NbO_x support. With regard to 0.8%Cu/Ti₂NbO_x, the peaks moved to higher binding energies slightly and became broader and weaker compared with those of 0.8%Cu/TiO₂. This indicates that the doping of niobium oxides facilitated the interaction of copper species and titanium, causing the decreasing of outer electron cloud density around Cu species.

The spectrum for the O 1s ionization was numerically fitted with two components. In Fig. 10(d), all the samples exhibited a primary peak at 529.77–530.75 eV assigning to be the lattice oxygen(O²⁻) (denoted as O_B) in metal oxides and a shoulder peak at 531.59–532.03 eV ascribed to surface chemisorbed oxygen species and weakly bonded oxygen species (denoted as O_A), such as O₂²⁻ and O⁻, belonging to defect-oxides or hydroxyl-like groups and chemisorbed water [39,40]. The surface oxygen (O_A) is regarded to be more reactive because of its higher mobility than lattice oxygen (O_B) [18,31,41]. The relative concentration ratios of O_A/(O_A+O_B) over each sample were calculated and the results were shown in Fig. 10(d) and Table 2. The proportion of O_A increased with the addition of niobium oxides and copper species. This might enhance the NO oxidation to NO₂ and facilitate the “fast-SCR” reaction leading to a higher catalytic activity [13,18,42]. It was implied that the addition of niobium oxides and copper species resulted in generating low-valence state metal cations than producing more oxygen vacancies, charge imbalances and unsaturated chemical bond on the surface of samples, which could absorb the chemisorbed oxygen and the weakly bonded oxygen species [17,43]. Compared with the TiO₂, the peak of O_B for Ti₂NbO_x shifted to higher energy as the niobium oxides had an effect on the oxygen atom of the TiO₂ lattice and might facilitate the redox cycle. In contrary, the peaks shifted to lower energy binding when copper species were added, especially for the 0.8%Cu/TiO₂, suggesting that the doping of copper species increased the extranuclear electron cloud in the oxygen atom of the supports [44], which might promote more surface oxygen existence to enhance NH₃-SCR activity.

3.2.3. The nature of copper species

In order to further investigate the nature of copper species over catalysts, both EPR and CO adsorption measurements were performed systematically.

In the forms of copper species, only isolated Cu²⁺ were characterized by EPR spectra while Cu⁺, CuO or binuclear species did not produce EPR signals [45,46]. Firstly, the spectra of TiO₂ and

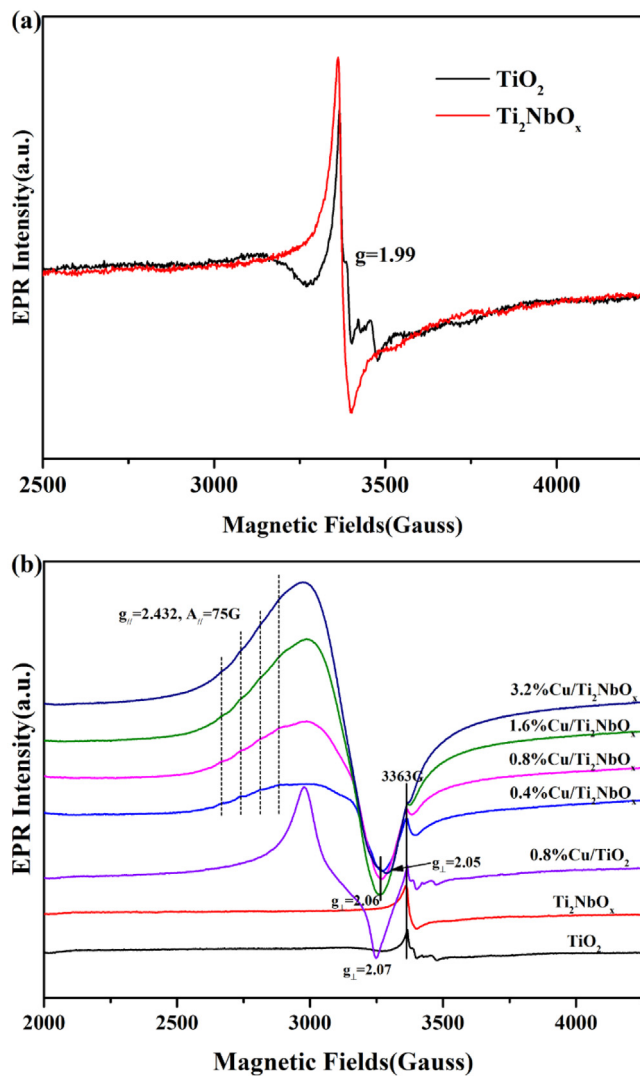


Fig. 11. EPR spectra of TiO_2 , Ti_2NbO_x , Cu/TiO_2 and $\text{Cu}/\text{Ti}_2\text{NbO}_x$ catalysts at 110 K.

Ti_2NbO_x were recorded, as shown in Fig. 11(a). Both of them exhibited TiO_2 phase with a g -value of 1.99, which was considered to be Ti^{3+} species [47,48]. Compared with TiO_2 , Ti_2NbO_x showed a single symmetrical signal, which was similar with the EPR results of Co-doped titanium dioxide nanobelts [49], indicating the effect of niobium oxides on TiO_2 . Then, a series of catalysts were tested under the same condition, as shown in Fig. 11(b). It was obvious that all the copper included samples had a spectral feature at 3363 G, which was the characteristic peak of TiO_2 or Ti_2NbO_x samples. Hyperfine structure could be observed at the parallel and perpendicular component of the spectra, illustrating the existence of isolated Cu^{2+} [30,50,51]. Interestingly, they were quite different from those of the Cu-molecular sieve catalysts. The profiles of $\text{Cu}/\text{Ti}_2\text{NbO}_x$ presented the hyperfine structure of isolated Cu^{2+} with $g_{||} = 2.432$, $A_{||} = 75$, $g_{\perp} = 2.05$ – 2.06 . Christoforidis [52] and Chary [53] attributed $g_{||} = 2.435$ and $A_{||} = 75$ to isolated copper ions incorporated in anatase matrix over CuVTi catalyst and $\text{Cu-TiO}_2\text{-ZrO}_2$ ternary catalyst, respectively. And Li [54] assigned the resonance parameters $g_{||} = 2.33$, $A_{||} = 100$, $g_{\perp} = 2.07$ to isolated Cu^{2+} ions at substitutional cation sites of TiO_2 in the CuO-TiO_2 samples. So, we believe that the isolated Cu^{2+} was mainly in a state of incorporating in anatase matrix over the $\text{Cu}/\text{Ti}_2\text{NbO}_x$ catalysts. Monotonic EPR signal intensity was enhanced with the increasing copper content. But the signals of hyperfine structure decreased, which could

Table 3
The amount of isolated Cu^{2+} ions based on EPR spectra.

Samples	Isolated Cu^{2+} (μmol)	Isolated Cu^{2+}/Cu species (%)
0.8%Cu/ TiO_2	0.477	22.36
0.4%Cu/ Ti_2NbO_x	0.552	39.98
0.8%Cu/ Ti_2NbO_x	0.698	49.83
1.6%Cu/ Ti_2NbO_x	2.448	48.95
3.2%Cu/ Ti_2NbO_x	4.782	47.82

be related with the dipole–dipole interaction between neighboring Cu^{2+} with some CuO clusters formed due to the increasing copper content [52]. For 0.8%Cu/ TiO_2 , hyperfine features at low field are barely detectable. It might be due to the small percentage of isolated Cu^{2+} in all the copper species, resulting a lower hyperfine resolution. Meanwhile, the signals of Ti^{3+} species decreased with the high copper loading. It was not clearly observed over 3.2%Cu/ Ti_2NbO_x and this was because the spectra was dominated by isolated Cu^{2+} ions.

Furthermore, five solutions of $\text{Cu}(\text{NO}_3)_2$ with known concentrations were measured to obtain the calibration curve. The EPR signals of Cu/TiO_2 and $\text{Cu}/\text{Ti}_2\text{NbO}_x$ catalysts were double-integrated, respectively. Then, the amount of isolated Cu^{2+} over the samples was calculated according to the obtained calibration curve. Also, the ratio of isolated Cu^{2+}/Cu species could be achieved. According to Table 3, the ratio of isolated Cu^{2+}/Cu species increased as the following sequence: 0.8%Cu/ TiO_2 < 0.4%Cu/ Ti_2NbO_x < 3.2%Cu/ Ti_2NbO_x < 1.6%Cu/ Ti_2NbO_x < 0.8%Cu/ Ti_2NbO_x . And 0.8%Cu/ Ti_2NbO_x had the highest ratio of isolated Cu^{2+}/Cu species than other samples, indicating the isolated Cu^{2+} ions played a significant role in the high $\text{NH}_3\text{-SCR}$ performance. The decrease of isolated Cu^{2+}/Cu species with the increasing Cu loading indicated the bulk CuO arose when more copper was doped. There were no characteristic peaks in the results of XRD, and it was probably because the nanocluster of CuO was not detectable by XRD [52]. The highest ratio of isolated Cu^{2+} ions in 0.8%Cu/ Ti_2NbO_x resulted in an excellent SCR activity, which was consistent with some previous findings [55,56].

Meanwhile, the CO adsorption results (Fig. 2S) showed non-isolated Cu^+ existed over both $\text{Cu}/\text{Ti}_2\text{NbO}_x$ and Cu/TiO_2 catalysts and the addition of niobium oxides enhanced the conversion of copper species into Cu^+ species. Therefore, the states of copper species were mainly isolated Cu^{2+} and non-isolated Cu^+ species over the 0.8%Cu/ Ti_2NbO_x catalyst from the results of EPR and in situ DRIFTS of CO adsorption.

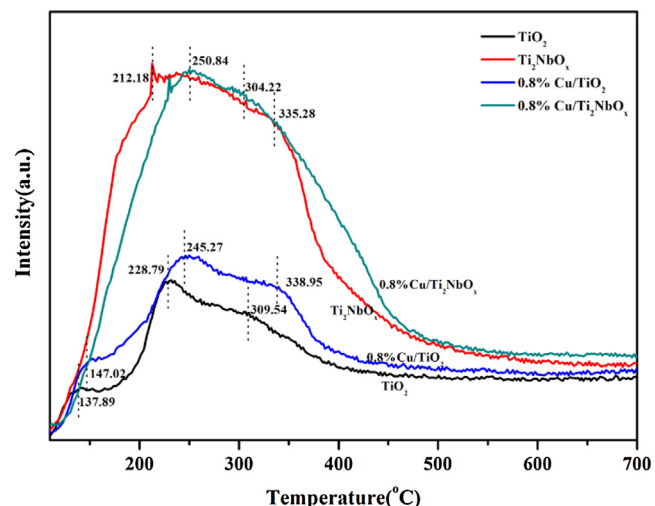


Fig. 12. $\text{NH}_3\text{-TPD}$ profiles of the samples: TiO_2 , Ti_2NbO_x , 0.8%Cu/ TiO_2 and 0.8%Cu/ Ti_2NbO_x .

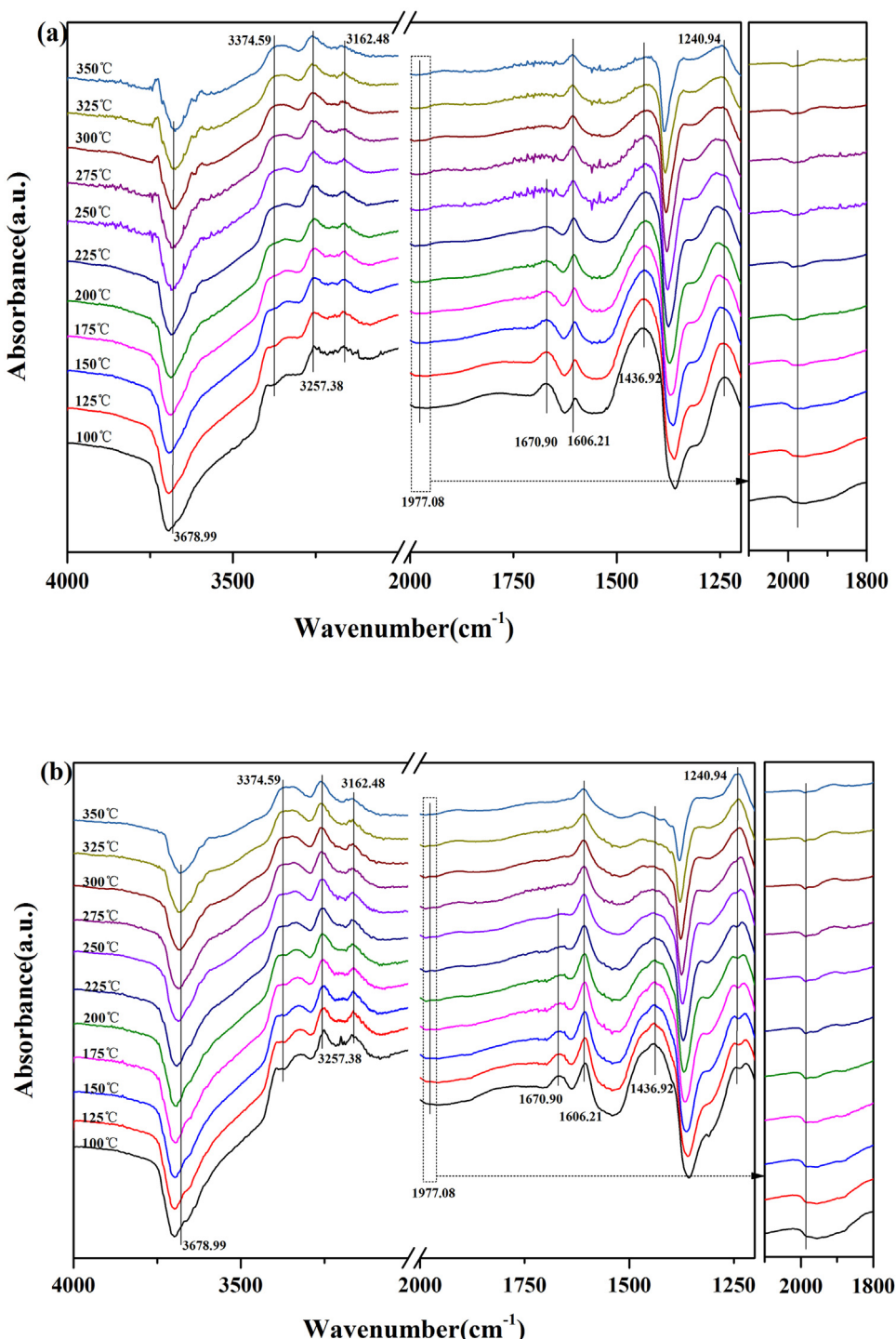


Fig. 13. In situ DRIFTS spectra of (a) Ti_2NbO_x and (b) 0.8%Cu/ Ti_2NbO_x pretreated in 1000 ppm NH_3/N_2 at 100 °C for 1 h and then purged by N_2 from 100 °C to 350 °C at a heating rate of 10 °C min⁻¹.

Table 4

H_2 consumption of samples measured by H_2 -TPR.

Samples	Reduction peaks temperature(°C)			The H_2 consumption(μmol/g)			Total H_2 consumption(μmol/g)
	α	β	γ	α	β	γ	
TiO_2	315	—	—	156.95	—	—	156.95
Ti_2NbO_x	344	572	758	48.207	228.27	899.72	1176.2
0.8%Cu/ Ti_2NbO_x	244	334	736	15.910	120.12	1020.1	1157.0
0.8%Cu/ TiO_2	198	421	585	109.93	466.38	117.57	693.89

3.2.4. Surface acid properties of the samples

The surface acidities of catalysts play a significant role in the NH₃-SCR reaction and it is chemically probed by chemisorption of basic NH₃ [57,58]. The NH₃-TPD experiment was carried out, as shown in Fig. 12. Three peaks appeared at below 150 °C, 150 °C–260 °C and above 260 °C were observed over TiO₂ and 0.8%Cu/TiO₂ while only two peaks centered at 200 °C–260 °C and above 300 °C were found for Ti₂NbO_x and 0.8%Cu/Ti₂NbO_x. The lower temperature desorption peaks below 260 °C were assigned to ammonium species adsorbed at weak acid sites with low thermal stability, whereas the high temperature desorption peak was attributed to ammonium species adsorbed at strong acid sites with high thermal stability [25]. It was obvious that the desorption peaks area followed the sequence of TiO₂ < 0.8%Cu/TiO₂ < Ti₂NbO_x < 0.8%Cu/Ti₂NbO_x. Clearly, increases in total amount of acid sites over Ti₂NbO_x were observed upon addition of niobium oxide, indicating the niobium oxide species could increase the catalyst surface acidity significantly due to its acid properties.

To investigate the NH₃ adsorption and desorption on the catalysts and distinguish the Brønsted acid sites and Lewis acid sites, *in situ* DRIFTS were conducted at 100 °C and the results were shown in Fig. 13. The bands at 1606 and 1241 cm⁻¹ were attributed to the asymmetric and symmetric bending vibrations N–H bonds in NH₃ coordinately linked to Lewis acid sites [5,59,60]. The bands at 1671 and 1437 cm⁻¹ could be ascribed to the asymmetric and symmetric bending vibrations of ionic NH₄⁺ species linked to Brønsted acid sites [4,13,61]. And the bands centered at around 3375, 3257 and 3162 cm⁻¹ were assigned to the N–H stretching vibrations coordinated NH₃ [4,10,18]. The negative bands around 3679 cm⁻¹ were ascribed to the consumption of surface hydroxyl groups (Nb–OH) by NH₃ to form NH₄⁺ [4,13]. Also, some negative bands around 1977 cm⁻¹ were attributed to the stretching mode of Nb=O in the overtone region, showing the consumption of Nb=O during the NH₃ adsorption [4]. The fundamental region of Nb=O stretching mode at 962–987 cm⁻¹ was not shown because of the overlap of the noises. The consumption of Nb-OH and Nb=O indicated that both of Nb-OH and Nb=O could act as acid sites during NH₃ adsorption. It has been reported in the literature that Nb-OH was related to Brønsted acid sites while Nb=O was responsible for Lewis acid sites [4,18]. So, the addition of niobium oxide species could increase Brønsted acid sites and Lewis acid sites, promoting the adsorption and activation of NH₃, which favored the SCR reaction. Meanwhile, the intensity of the band at 1671 cm⁻¹ diminished with the increase of temperature and vanished at 250 °C for Ti₂NbO_x and 0.8%Cu/Ti₂NbO_x. At the same time, the intensity of the band at 1437 cm⁻¹ decreased, indicating that the ionic NH₄⁺ species linked to Brønsted acid sites had less thermal stability. Therefore, the Brønsted acid sites might contribute to relatively lower temperature reaction. Furthermore, the intensity of the band at 1241 cm⁻¹ decreased slightly while it almost kept the same for the band at 1606 cm⁻¹, indicating that the NH₃ species coordinated on Lewis acid sites had better thermal stability. This showed that Lewis acid sites might contribute to both low and high temperature reaction. Hence, from *in situ* DRIFTS of NH₃ adsorption and desorption, we can draw a conclusion that the peaks of NH₃-TPD below 300 °C mainly stand for Brønsted acid sites and Lewis acid sites while the peak higher than 300 °C is mainly denoted as Lewis acid sites. And doping niobium oxide could effectively enhance Lewis acid sites and Brønsted acid sites of the support, which would lead to more NH₃ adsorbed on the surface of the catalyst.

3.2.5. Redox properties of the samples

Hydrogen temperature programmed reduction (H₂-TPR) is widely applied for analyzing the reduction properties of chemical substances. It is a method probing into the source of oxygen species

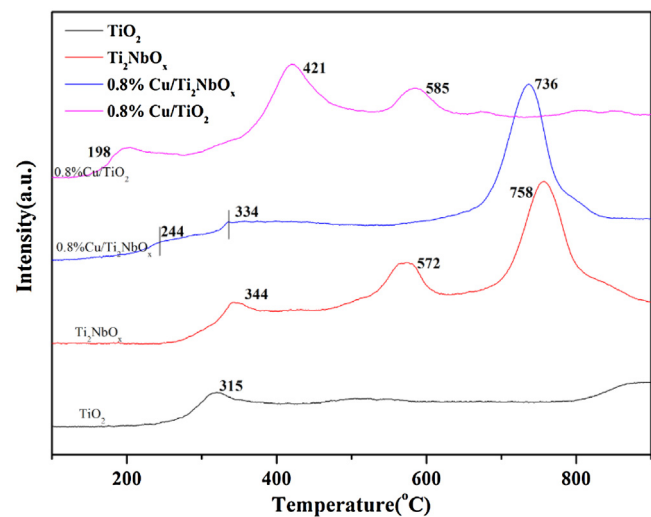


Fig. 14. H₂-TPR curves of TiO₂, Ti₂NbO_x, 0.8%Cu/TiO₂ and 0.8%Cu/Ti₂NbO_x catalysts.

of materials with the hydrogen as a probe molecule. The hydrogen reacted with different states of oxygen with the increase of temperature. Meanwhile, the reaction temperature of hydrogen reduction and the consumption of hydrogen would be recorded by the detector. The reducibility of chemical substances would be studied by the reduction temperature and hydrogen consumption.

The reducibility of catalysts was studied by H₂-TPR experiment, as shown in Fig. 14. TiO₂ showed a stage of reduction at 315 °C, caused by the reduction of surface TiO₂ [5]. Interestingly, Ti₂NbO_x support showed three reduction peaks. The peaks at 344 °C and 572 °C were associated with the reduction of surface capping oxygen promoted by niobium oxide modification [4,28]. The broad peak at 758 °C was responsible for the reduction of Nb₂O₅ to Nb₂O₄ [62–64]. The reduction peaks shifted to low-temperature after copper oxide doping, indicating that the incorporation of copper oxide could promote the reduction of Ti₂NbO_x. As for 0.8%Cu/TiO₂, the peak at 198 °C was assigned to the reduction of Cu²⁺ to Cu⁺ [65], while the second and third peaks were as related to the reduction of Cu⁺ to copper metallic [46,66]. The Cu⁺ was partly from the reduction of isolated Cu²⁺ and partly from the original Cu⁺ existing on the catalyst [46,67]. The peak at high temperature (585 °C) was because of the highly stable Cu⁺. There were also three peaks about the 0.8%Cu/Ti₂NbO_x. The first peak at 244 °C was attributed to the reduction of isolated Cu²⁺ to Cu⁺ and the second peak at 344 °C was attributed to the reduction of Cu⁺ to copper metallic [25,68]. Compared with 0.8%Cu/TiO₂, the temperature of copper species reduction was lower for 0.8%Cu/Ti₂NbO_x and the Cu⁺ was much easier to be reduced, which indicated that the 0.8%Cu/Ti₂NbO_x had an excellent reducibility. And the amount of H₂ consumption was shown in Table 4. The H₂ consumption increased as the following sequence: TiO₂ < 0.8%Cu/TiO₂ < Ti₂NbO_x ≈ 0.8%Cu/Ti₂NbO_x. It was obvious that H₂ consumption of Ti₂NbO_x and 0.8%Cu/Ti₂NbO_x were larger than those of TiO₂ and 0.8%Cu/TiO₂, suggesting that addition of niobium oxides and copper oxides could result in a higher redox capability and further leading to a better catalytic activity within the temperature investigated.

3.3. Reaction mechanism

To investigate the formation and transformation of surface adsorbed species in the NH₃-SCR reaction on the 0.8%Cu/Ti₂NbO_x catalyst, *in situ* DRIFTS were recorded as a function of time at the reaction temperature of 225 °C, where the NO_x conversion was 79%. When the sample was saturated by the adsorbed NH₃

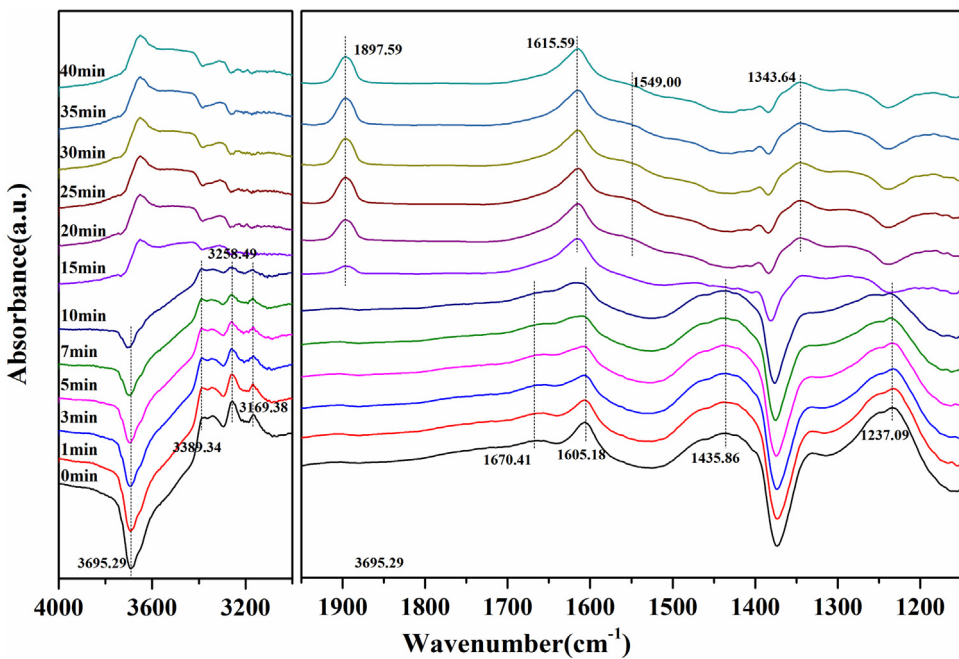


Fig. 15. In situ DRIFTS of gaseous NO and O₂ reacted with pre-adsorbed NH₃ species over 0.8%Cu/Ti₂NbO_x catalyst at 225 °C. Reaction conditions: [NH₃] = 1000 ppm (when used), [NO] = 1000 ppm (when used), [O₂] = 5%, total flow rate = 100 mL min⁻¹ and N₂ as balance.

species and purged with N₂ (Fig. 15), coordinated NH₃ on Lewis acid sites (1605 cm⁻¹ and 1237 cm⁻¹) and NH₄⁺ bound to Brønsted acid sites (1670 cm⁻¹ and 1436 cm⁻¹) were observed [13,69,70]. Then NO and O₂ were introduced and the N–H stretching vibrations coordinated NH₃ (3389 cm⁻¹, 3258 cm⁻¹ and 3169 cm⁻¹), coordinated NH₃ on Lewis acid sites (1605 cm⁻¹ and 1237 cm⁻¹) and NH₄⁺ bound to Brønsted acid sites (1670 cm⁻¹ and 1436 cm⁻¹) were gradually consumed and replaced by the surface nitrate species after 15 min. Hence, it indicated both coordinated NH₃ and ionic NH₄⁺ were active intermediates over 0.8%Cu/Ti₂NbO_x catalyst, which was in consistence with some conventional catalysts, such as Cu/SSZ-13 [71], Mn₂Nb₁O_x [18], WO₃–CeO₂ [72], Ce_{0.2}W_{0.2}TiO_x [13] catalysts. The addition of niobium oxides on 0.8%Cu/Ti₂NbO_x resulted in more acid sites including Lewis acid sites and Brønsted acid sites than 0.8%Cu/TiO₂, and the increasing of acid sites favored the catalytic activity. After 15 min, new nitrate peaks assigned to monodentate nitrates (1344 cm⁻¹) and bidentate nitrate (1549 cm⁻¹) emerged [13,71,73,74]. Meanwhile, the adsorbed NO species exhibited a peak at 1898 cm⁻¹ [5,69]. For the band at 1616 cm⁻¹, Liu et al. [75] assigned the band at 1613 cm⁻¹ to NO + O₂ adsorption over V₂O₅–CeO₂/TiO₂ catalyst and Hu et al. [76] attributed the band at 1616 cm⁻¹ to adsorbed NO₂ on their V–Ce(SO₄)₂/Ti. Otherwise, the bands at 1620 cm⁻¹ were assigned to the bridging nitrates over Cu-CHA catalyst by Ruggieri et al. [77]. In this research, we also attributed the bands at 1616 cm⁻¹ to the bridging nitrates as both Cu-CHA and 0.8%Cu/Ti₂NbO_x catalysts belonged to Cu-based catalyst and the results would be more reasonable.

Meanwhile, the normalized peak areas at the bands of 1898 cm⁻¹, 1616 cm⁻¹, 1344 cm⁻¹, 1436 cm⁻¹ and 1237 cm⁻¹ were calculated to more clearly demonstrate the evolution of intermediates in the reaction, since the bands at 1670 cm⁻¹ and 1549 cm⁻¹ were so slight that could be effect by the noise and the bands at 1605 cm⁻¹ were overlapped by the bands at 1616 cm⁻¹. As shown in Fig. 16, both coordinated NH₃ and ionic NH₄⁺ decreased almost simultaneously and disappeared in 15 min. At the same time, monodentate nitrates, bridging nitrates and adsorbed NO species appeared and increased with different rate. Bridging nitrates

increased to the maximum at the first in all of nitrate species, indicating bridging nitrates was the most easily generated species over 0.8%Cu/Ti₂NbO_x catalysts when exposing to the atmosphere of NO and O₂. In this part, we could conclude the Eley-Rideal (E-R) mechanism occurred on the catalyst.

The reaction between NH₃ and pre-adsorbed NO_x deriving from NO and O₂ co-adsorption was conducted at 225 °C, as shown in Fig. 17. After NO_x was saturated then purged with N₂ for about 30 min, the peaks assigned to bridging nitrate at 1615 cm⁻¹, monodentate nitrates at 1345 cm⁻¹ and bidentate nitrates at 1545 cm⁻¹ were displayed, respectively [5,74]. Afterwards, NH₃ and O₂ were introduced. All of the nitrates diminished and the ad-NH₃ species at 3386 cm⁻¹, 3258 cm⁻¹, 3166 cm⁻¹, 1606 cm⁻¹, 1670 cm⁻¹, 1435 cm⁻¹ and 1229 cm⁻¹ appeared after 1 min, indicating that monodentate nitrates, bidentate nitrates and bridging nitrates were involved in the reaction over this catalyst, which was really different from some previous investigations. Lian et al. [18] found NH₃ could react with bridging nitrates and monoden-

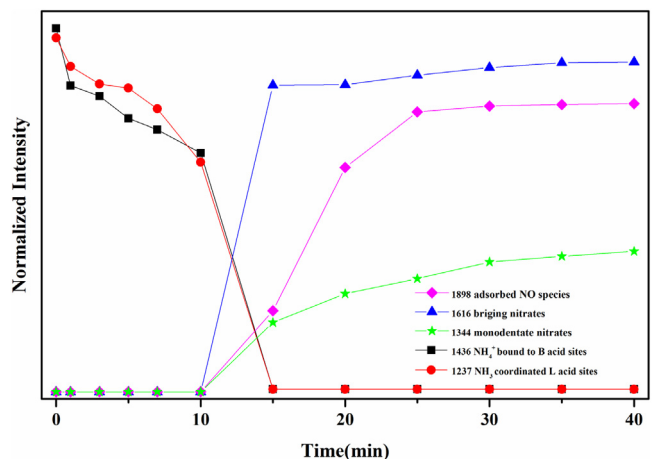


Fig. 16. Normalized in situ DRIFTS peaks intensity during the reaction between NO + O₂ and pre-adsorbed NH₃ species over 0.8%Cu/Ti₂NbO_x catalyst at 225 °C.

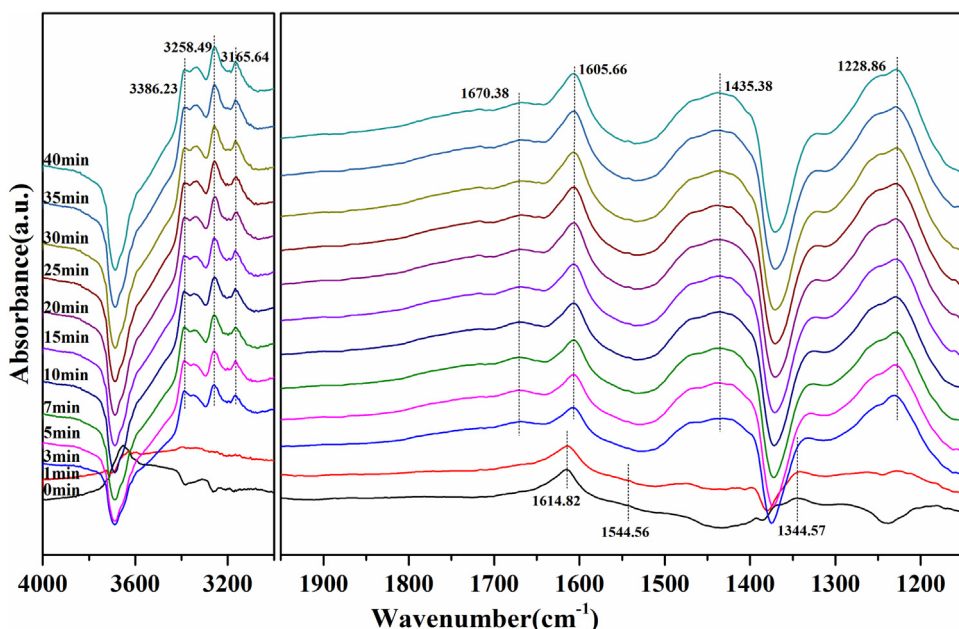


Fig. 17. In situ DRIFTS of gaseous NH₃ and O₂ reacted with pre-adsorbed NO + O₂ species over 0.8%Cu/Ti₂NbO_x catalyst at 225 °C. Reaction conditions: [NH₃] = 1000 ppm (when used), [NO] = 1000 ppm (when used), [O₂] = 5%, total flow rate = 100 mL min⁻¹ and N₂ as balance.

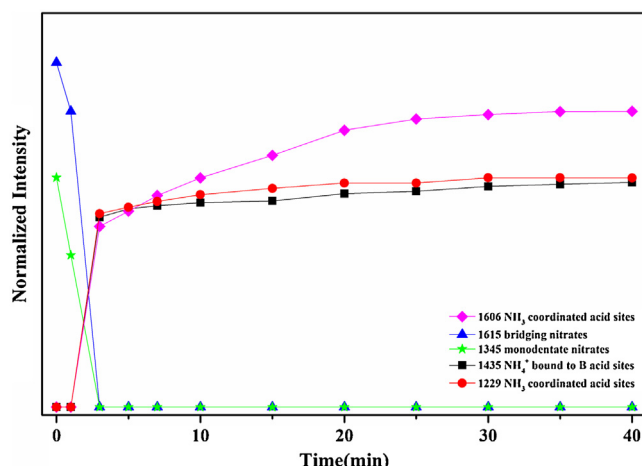


Fig. 18. Normalized in situ DRIFTS peaks intensity during the reaction between NH₃ and pre-adsorbed NO + O₂ species over 0.8%Cu/Ti₂NbO_x catalyst at 225 °C.

tate nitrates, but not bidentate nitrates on the Mn₂Nb₁O_x catalyst. Qu et al. [78] proposed only monodentate nitrates participated in the NH₃-SCR reaction over cerium–niobium oxide catalysts while bidentate nitrates and bridging nitrates remained stable in the reaction due to their high thermal stability. Meanwhile, the normalized peak areas at the bands of 1606 cm⁻¹, 1615 cm⁻¹, 1345 cm⁻¹, 1435 cm⁻¹ and 1229 cm⁻¹ were calculated, as shown in Fig. 18. It was obvious that bridging nitrates and monodentate nitrates were consumed then coordinated NH₃ and ionic NH₄⁺ began to produce at a different rate. However, the transition of nitrates and gaseous NH₃ was so fast within 3–5 min and the spectra were difficult to be recorded clearly since the number of scans was 64. In this part, we could conclude the Langmuir–Hinshelwood (H-L) mechanism occurred on the catalyst from the experiment. Compared with the results presented in Fig. 16, both the Eley–Rideal (E-R) mechanism and Langmuir–Hinshelwood (H-L) mechanism occurred in the NH₃-SCR reaction over 0.8%Cu/Ti₂NbO_x catalyst at 225 °C.

4. Conclusions

In this work, a series of titanium–niobium binary oxide as catalyst support were synthesized by co-precipitation. Ti₂NbO_x exhibited an optimal activity with 96% of NO_x conversion and 98% of N₂ selectivity within 400–450 °C. Then Ti₂NbO_x was selected as support for further experiments and different amount of copper was doped by wetness impregnation method to further increase the catalytic activity. Furthermore, 0.8%Cu/TiO₂ was also prepared by the same method for comparison. Among the catalysts, 0.8%Cu/Ti₂NbO_x showed excellent NH₃-SCR with over 90% of NO_x conversion and 97% of N₂ selectivity in a wide temperature range from 250 °C to 425 °C under a high GHSV of 17,7000 h⁻¹. Besides, water vapor or/and SO₂ had a slightly reversible inhibition influence on the catalytic performance over 0.8%Cu/Ti₂NbO_x, and it exhibited an excellent hydrothermal stability. Meanwhile, an array of analytical techniques were employed to investigate the Micro-morphology, structure, surface acid property, redox property and reaction mechanism of the catalysts. Several conclusions based on the above-mentioned characterization can be drawn as below.

- (1) The introduction of niobium oxide results in a larger specific surface area compared with that of single anatase TiO₂. Also, it inhibits the growth of anatase TiO₂, leading to a decrease of the crystallite size. Both of them are favored of dispersion of the copper species on the support, being advantageous to the NH₃-SCR reaction.
- (2) The copper species are mainly in the state of isolated Cu²⁺ and non-isolated Cu⁺ over the 0.8%Cu/Ti₂NbO_x catalyst. And the highest ratio of isolated Cu²⁺/Cu species results in an excellent NH₃-SCR performance of 0.8%Cu/Ti₂NbO_x catalyst.
- (3) Addition of niobium oxide enhances the total acidity of the catalyst, promoting the NH₃ adsorption and preventing the selective oxidation of NH₃. The amount of surface oxygen on catalyst is increased upon niobium oxide doping and the redox capability is promoted by niobium oxide and copper oxides, which indicate a promotional synergistic effect of copper and niobium in 0.8%Cu/Ti₂NbO_x catalyst. Abundant acid sites, sur-

- face adsorbed oxygen and redox capability give rise to a better catalytic performance for 0.8%Cu/Ti₂NbO_x catalyst.
- (4) The reaction of 0.8%Cu/Ti₂NbO_x ternary oxide catalyst follows both the Eley-Rideal (E-R) mechanism and Langmuir-Hinshelwood (H-L) mechanism at 225 °C. Moreover, both coordinated NH₃ and ionic NH₄⁺ are active intermediates and monodentate nitrates, bidentate nitrates and bridging nitrates are involved in the reaction over 0.8%Cu/Ti₂NbO_x catalyst at the reaction temperature of 225 °C.

Acknowledgements

The authors would like to gratefully acknowledge the financial support from the National Natural Science Foundation of China (NO. 21606195) and the Natural Science Fund of Zhejiang Province, China (NO. LQ14B060006).

Appendix A. Supplementary data

Supplementary data associated with this article can be found, in the online version, at <http://dx.doi.org/10.1016/j.apcatb.2017.08.021>.

References

- [1] Y. Shi, Y.F. Xia, B.H. Lu, N. Liu, L. Zhang, S.J. Li, W. Li, *J. Zhejiang Univ. Sci. A* 15 (2014) 454–464.
- [2] W. Li, S. Tan, Y. Shi, S.J. Li, *Fuel* 160 (2015) 35–42.
- [3] Y. Shi, S. Tan, S.J. Li, J.K. Zhao, Y.F. Xia, B.H. Lv, W. Li, *Catal. Sci. Technol.* 5 (2015) 3613–3623.
- [4] R.Y. Qu, X. Gao, K.F. Cen, J.H. Li, *Appl. Catal. B: Environ.* 142 (2013) 290–297.
- [5] X.J. Yao, L. Zhang, L.L. Li, L.C. Liu, Y. Cao, X. Dong, F. Gao, Y. Deng, C.J. Tang, Z. Chen, L. Dong, Y. Chen, *Appl. Catal. B: Environ.* 150 (2014) 315–329.
- [6] C. Liu, L. Chen, J. Li, L. Ma, H. Arandiyani, Y. Du, J. Xu, J. Hao, *Environ. Sci. Technol.* 46 (2012) 6182–6189.
- [7] M. Moliner, C. Franch, E. Palomares, M. Grill, A. Corma, *Chem. Commun.* 48 (2012) 8264–8266.
- [8] G. Busca, L. Lietti, G. Ramis, F. Berti, *Appl. Catal. B: Environ.* 18 (1998) 1–36.
- [9] Y. Shi, S. Tan, X.X. Wang, M.F. Li, S.J. Li, W. Li, *Catal. Commun.* 86 (2016) 67–71.
- [10] N.Y. Topsoe, *Science* 265 (1994) 1217–1219.
- [11] J.A. Sullivan, *Catal. Lett.* 79 (2002) 59–62.
- [12] Y. Yu, J. Chen, J. Wang, Y. Chen, *Chin. J. Catal.* 37 (2016) 281–287.
- [13] W.P. Shan, F.D. Liu, H. He, X.Y. Shi, C.B. Zhang, *Appl. Catal. B: Environ.* 115 (2012) 100–106.
- [14] K. Zhao, W. Han, G. Lu, J. Lu, Z. Tang, X. Zhen, *Appl. Surf. Sci.* 379 (2016) 316–322.
- [15] K.A. Vikulov, A. Andreini, E.K. Poels, A. Bliek, *Catal. Lett.* 25 (1994) 49–54.
- [16] S. Okazaki, H. Kuroha, T. Okuyama, *Chem. Lett.* 14 (1985) 45–48.
- [17] Z.R. Ma, X.D. Wu, Z.C. Si, D. Weng, J. Ma, T.F. Xu, *Appl. Catal. B: Environ.* 179 (2015) 380–394.
- [18] Z.H. Lian, F.D. Liu, H. He, X.Y. Shi, J.S. Mo, Z.B. Wu, *Chem. Eng. J.* 250 (2014) 390–398.
- [19] Z. Si, D. Weng, X. Wu, J. Li, G. Li, *J. Catal.* 271 (2010) 43–51.
- [20] A.M. Beale, F. Gao, I. Lpezcano-Gonzalez, C.H.F. Peden, J. Szanyi, *Chem. Soc. Rev.* 44 (2015) 7371–7405.
- [21] S. Prodinger, M.A. Derewinski, Y. Wang, N.M. Washton, E.D. Walter, J. Szanyi, F. Gao, Y. Wang, C.H.F. Peden, *Appl. Catal. B: Environ.* 201 (2017) 461–469.
- [22] D. Pietrogiacomi, D. Sannino, A. Magliano, P. Ciambelli, S. Tuti, V. Indovina, *Appl. Catal. B: Environ.* 36 (2002) 217–230.
- [23] S. Prodinger, M.A. Derewinski, Y.L. Wang, N.M. Washton, E.D. Walter, J. Szanyi, F. Gao, Y. Wang, C.H.F. Peden, *Appl. Catal. B: Environ.* 201 (2017) 461–469.
- [24] F. Gao, E.D. Walter, E.M. Karp, J. Luo, R.G. Tonkyn, J.H. Kwak, J. Szanyi, C.H.F. Peden, *J. Catal.* 300 (2013) 20–29.
- [25] L. Wang, W. Li, S.J. Schmiege, D. Weng, *J. Catal.* 324 (2015) 98–106.
- [26] L.M. Yu, Q. Zhong, S.L. Zhang, W. Zhao, R. Zhang, *Combust. Sci. Technol.* 187 (2015) 925–936.
- [27] L.J. Xie, F.D. Liu, X.Y. Shi, F.S. Xiao, H. He, *Appl. Catal. B: Environ.* 179 (2015) 206–212.
- [28] D.S. Zhou, Z.Y. Ren, B. Li, Z.X. Ma, X.B. Zhang, H.S. Yang, *RSC Adv.* 5 (2015) 31708–31715.
- [29] J. Wang, Y. Huang, T. Yu, S.C. Zhu, M.Q. Shen, W. Li, J.Q. Wang, *Catal. Sci. Technol.* 4 (2014) 3004–3012.
- [30] T. Yu, J. Wang, Y. Huang, M.Q. Shen, W. Li, J.Q. Wang, *ChemCatChem* 6 (2014) 2074–2083.
- [31] X.S. Du, X. Gao, Y.C. Fu, F. Gao, Z.Y. Luo, K.F. Cen, *J. Colloid Interface Sci.* 368 (2012) 406–412.
- [32] L.J. Alemany, F. Berti, G. Busca, G. Ramis, D. Robba, G.P. Toledo, M. Trombetta, *Appl. Catal. B: Environ.* 10 (1996) 299–311.
- [33] Z.M. Liu, Y. Yi, J.H. Li, S.I. Woo, B.Y. Wang, X.Z. Cao, Z.X. Li, *Chem. Commun.* 49 (2013) 7726–7728.
- [34] Q.Q. Hu, J.Q. Huang, G.J. Li, Y.B. Jiang, H. Lan, W. Guo, Y.G. Cao, *Appl. Surf. Sci.* 382 (2016) 170–177.
- [35] J. Fang, X.Z. Bi, D.J. Si, Z.Q. Jiang, W.X. Huang, *Appl. Surf. Sci.* 253 (2007) 8952–8961.
- [36] G.S. Qi, R.T. Yang, *Appl. Catal. B: Environ.* 44 (2003) 217–225.
- [37] D.S. Zhou, B. Li, Z.X. Ma, X.D. Huang, X.B. Zhang, H.S. Yang, *J. Mol. Catal. A: Chem.* 409 (2015) 183–190.
- [38] B. Li, Z.Y. Ren, Z.X. Ma, X.D. Huang, F. Liu, X.B. Zhang, H.S. Yang, *Catal. Sci. Technol.* 6 (2016) 1719–1725.
- [39] Z.B. Wu, R.B. Jin, Y. Liu, H.Q. Wang, *Catal. Commun.* 9 (2008) 2217–2220.
- [40] T.T. Gu, Y. Liu, X.L. Weng, H.Q. Wang, Z.B. Wu, *Catal. Commun.* 12 (2010) 310–313.
- [41] H. Chen, A. Sayari, A. Adnot, F. Larachi, *Appl. Catal. B: Environ.* 32 (2001) 195–204.
- [42] M. Kang, E.D. Park, J.M. Kim, J.E. Yie, *Appl. Catal. A: Gen.* 327 (2007) 261–269.
- [43] X. Gao, Y. Jiang, Y. Zhong, Z.Y. Luo, K.F. Cen, *J. Hazard. Mater.* 174 (2010) 734–739.
- [44] F.D. Liu, H. He, C.B. Zhang, Z.C. Feng, L.R. Zheng, Y.N. Xie, T.D. Hu, *Appl. Catal. B: Environ.* 96 (2010) 408–420.
- [45] J. Xue, X. Wang, G. Qi, J. Wang, M. Shen, W. Li, *J. Catal.* 297 (2013) 56–64.
- [46] X.S. Liu, X.D. Wu, D. Weng, Z.C. Si, R. Ran, *Catal. Today* 281 (2017) 596–604.
- [47] E.A. Reyes-Garcia, Y. Sun, K.R. Reyes-Gil, D. Raftery, *Solid State Nucl. Magn. Reson.* 35 (2009) 74–81.
- [48] J. Soria, J. Sanz, I. Sobrados, J.M. Coronado, F. Fresno, M.D. Hernández-Alonso, *Catal. Today* 129 (2007) 240–246.
- [49] S.V. Chong, J. Xia, N. Suresh, K. Yamaki, K. Kadokawa, *Solid State Commun.* 148 (2008) 345–349.
- [50] E. Bozkurt, A. Döner, I. Uçar, B. Karabulut, *Chem. Phys. Lett.* 502 (2011) 163–168.
- [51] F. Giordanino, P.N.R. Vennestrøm, L.F. Lundegaard, F.N. Stappen, S. Mossin, P. Beato, S. Bordiga, C. Lamberti, *Dalton Trans.* 42 (2013) 12741–12761.
- [52] K.C. Christoforidis, M.F. Garcia, *Catal. Sci. Technol.* 6 (2016) 1094–1105.
- [53] K.V.R. Chary, G.V. Sagar, D. Naresh, K.K. Seela, B. Sridhar, *J. Phys. Chem. B* 109 (2005) 9437–9444.
- [54] G. Li, N.M. Dimitrijevic, C. Le, T. Rajh, K.A. Gray, *J. Phys. Chem. C* 112 (2011) 19040–19044.
- [55] Q. Guo, F. Fan, D.A.J.M. Ligthart, G. Li, D.Z. Feng, D.C. Li, *ChemCatChem* 6 (2014) 634–639.
- [56] T. Zhang, F. Qiu, H. Chang, X. Li, J. Li, *Catal. Sci. Technol.* 6 (2016).
- [57] L. Lietti, J.L. Alemany, P. Forzatti, G. Busca, G. Ramis, E. Giamello, F. Bregani, *Catal. Today* 29 (1996) 143–148.
- [58] J.M.G. Amores, V.S. Escribano, G. Ramis, G. Busca, *Appl. Catal. B: Environ.* 13 (1997) 45–58.
- [59] T.T. Gu, R.B. Jin, Y. Liu, H.F. Liu, X.L. Weng, Z.B. Wu, *Appl. Catal. B: Environ.* 129 (2013) 30–38.
- [60] G. Ramis, M.A. Larrubia, *J. Mol. Catal. A: Chem.* 215 (2004) 161–167.
- [61] S.J. Yang, C.Z. Wang, J.H. Li, N.Q. Yan, L. Ma, H.Z. Chang, *Appl. Catal. B: Environ.* 110 (2011) 71–80.
- [62] I.E. Wachs, L.E. Briand, J.M. Jehng, L. Burcham, X.T. Gao, *Catal. Today* 57 (2000) 323–330.
- [63] A.E. Lewandowska, M.A. Banares, *Catal. Today* 118 (2006) 323–331.
- [64] S. Pengpanich, V. Meeyoo, T. Rirkosboon, J. Schwank, *J. Nat. Gas Chem.* 16 (2007) 227–234.
- [65] L. Wang, W. Li, G.S. Qi, D. Weng, *J. Catal.* 289 (2012) 21–29.
- [66] M. Richter, M.J.G. Fait, R. Eckelt, M. Schneider, J. Radnik, D. Heidemann, R. Fricke, *J. Catal.* 245 (2007) 11–24.
- [67] S. Han, Q. Ye, S.Y. Cheng, T.F. Kang, H.X. Dai, *Catal. Sci. Technol.* 7 (2017) 703–717.
- [68] F. Gao, E.D. Walter, N.M. Washton, J. Szanyi, C.H.F. Peden, *Appl. Catal. B: Environ.* 162 (2015) 501–514.
- [69] Z.G. Xie, X.X. Zhou, H.X. Wu, L.S. Chen, H. Zhao, Y. Liu, L.Y. Pan, H.R. Chen, *Sci. Rep. UK* 6 (2016).
- [70] W.S. Hu, X. Gao, Y.W. Deng, R.Y. Qu, C.H. Zheng, X.B. Zhu, K.F. Cen, *Chem. Eng. J.* 293 (2016) 118–128.
- [71] W.K. Su, H.Z. Chang, Y. Peng, C.Z. Zhang, J.H. Wi, *Environ. Sci. Technol.* 49 (2015) 467–473.
- [72] S. Zhan, H. Zhang, Y. Zhang, Q. Shi, Y. Li, X. Li, *Appl. Catal. B: Environ.* 203 (2017) 199–209.
- [73] J. Liu, X.Y. Li, Q.D. Zhao, C. Hao, D.K. Zhang, *Environ. Sci. Technol.* 47 (2013) 4528–4535.
- [74] J. Liu, X.Y. Li, Q.D. Zhao, J. Ke, H.N. Xiao, X.J. Lv, S.M. Liu, M. Tade, S.B. Wang, *Appl. Catal. B: Environ.* 200 (2017) 297–308.
- [75] Z. Liu, S. Zhang, J. Li, J. Zhu, L. Ma, *Appl. Catal. B: Environ.* 158–159 (2014) 11–19.
- [76] W.S. Hu, Y.H. Zhang, S.J. Liu, C.H. Zheng, X. Gao, I. Nova, E. Tronconi, *Appl. Catal. B: Environ.* 206 (2017) 449–460.
- [77] M.P. Ruggeri, I. Nova, E. Tronconi, J.A. Pihl, T.J. Toops, W.P. Partridge, *Appl. Catal. B: Environ.* 166–167 (2015) 181–192.
- [78] R. Qu, Y. Peng, X. Sun, J. Li, X. Gao, K. Cen, *Catal. Sci. Technol.* 6 (2016) 2136–2142.